2009

Quantifying the Effects of Cementation on the Hydromechanical Properties of Granular Porous Media Using Discrete Element and Poroelastic Models

Kathleen E. Plourde
University of Massachusetts Amherst

QUANTIFYING THE EFFECTS OF CEMENTATION ON THE HYDROMECHANICAL PROPERTIES OF GRANULAR POROUS MEDIA USING DISCRETE ELEMENT AND POROELASTIC MODELS

A Thesis Presented

by

KATHLEEN E. PLOURDE

Submitted to the Graduate School of the
University of Massachusetts Amherst in partial fulfillment
of the requirements for the degree of

MASTER OF SCIENCE

February 2009

Geosciences

QUANTIFYING THE EFFECTS OF CEMENTATION ON THE HYDROMECHANICAL PROPERTIES OF GRANULAR POROUS MEDIA USING DISCRETE ELEMENT MODELS AND POROELASTIC MODELS

A Thesis Presented

by

KATHLEEN E. PLOURDE

Approved as to style and content by:

_____
David F. Boutt, Chair

_____
Michele L. Cooke, Member

_____
Stephen B. Mabee, Member

_____
Michael Williams, Department Head

DEDICATION

This manuscript is dedicated to Mark, Laurie, Rachel and Jason for their devoted support and eternal patience.

I would also like to dedicate this work to my mother and sister, for the sacrifices we all have made.

ACKNOWLEDGMENTS

I would like to sincerely thank my advisor, David F. Boutt, for his guidance and patience during this research. He accomplished the daunting task of expanding my understanding and appreciation of computer models. I would also like to acknowledge our collaborators, Laurel B. Goodwin and Jennie Cook at the University of Wisconsin, Madison and Thomas E. Buchheit at Sandia National Laboratories for their invaluable contributions of knowledge from multiple disciplines that truly enriched this project.

I would like to thank my committee members, Michele Cooke and Stephen Mabee, and the Research In Progress group for helping mold this work with essential comments and insight.

Finally, I would like to acknowledge the Department of Energy, Basic Energy Sciences, Geosciences Award # DE-FG02-05ER15740 for funding this research.

ABSTRACT

QUANTIFYING THE EFFECTS OF CEMENTATION ON THE HYDROMECHANICAL PROPERTIES OF GRANULAR POROUS MEDIA USING DISCRETE ELEMENT MODELS AND POROELASTIC MODELS

FEBRUARY 2009

KATHLEEN E. PLOURDE, B.A., HARTWICK COLLEGE

M.A., UNIVERSITY OF MASSACHUSETTS AMHERST

Directed by: Professor David F. Boutt

Cementation is known to significantly influence the mechanical and hydrologic properties of granular porous media by increasing the stiffness of the elastic response to stress and reducing permeability. The relationship between the changes in cementation and changes in permeability are well documented in literature. However, limited quantitative data exists on the relationship between changes in the amount of cementation and changes in the mechanical response of granular media. The goal of this research is to quantify the effects of cementation on the mechanical properties of granular porous media at the meso-scale and investigate the influence of the competing roles of mechanical and hydrologic properties on fluid flow and deformation at the macro-scale. To accomplish this goal, we developed a multiple scale approach that utilizes the parameterization control of meso-scale Discrete Element Method (DEM) models and the ability to couple fluid flow and solid deformation physics with macro-scale poro-elasticity models.

At the meso-scale, a series of DEM models are designed to simulate biaxial tests of variably cemented sandstone in order to investigate the effects of cementation on the elastic and inelastic response of the porous media. The amount of cementation in the DEM model is quantified using a bond to grain ratio (BGR). The BGR is the number of bonds (the bonds represent the cement) divided by the number of grains in each model. The BGRs of the DEM models correlate to BGRs of natural samples and allow constraint of the percent cementation in the DEM models. A decrease in BGR from 2.25 to 1.00 results in a 1.4 fold decrease in shear modulus. The resulting shear moduli from the DEM models are used as input properties into two dimensional, axial symmetric poroelastic models of an isotropic confined aquifer. The poroelastic models address the implications of changes in mechanical properties and hydrologic properties on large scale fluid removal and deformation as well as address the importance of the competing roles of hydrologic and mechanical properties.

TABLE OF CONTENTS

Page

LIST OF TABLES

LIST OF FIGURES

Figure

CHAPTER 1

INTRODUCTION

In recent years, population growth, climate change and surface water contamination have caused a significant increase in the development of groundwater resources. Groundwater is a crucial source of fresh water throughout the world for drinking, agriculture and industrial purposes. According to Alley et al. (2002) more than 50% of the population of the United States and over 1.5 billion people worldwide rely on groundwater for their primary source of drinking water. However, in many areas around the world, the demand on groundwater resources has caused the rate of groundwater use to exceed the rate of groundwater replenishment, resulting in groundwater depletion. As the fluid pressure declines in an aquifer from fluid withdrawal, the effective stress on the granular skeleton of the aquifer increases and causes the granular skeleton to contract. Assuming the skeletal contraction is within the limits of the elastic compressibility of the granular skeleton, the granular skeleton will rebound to its pre-compaction state once the fluid pressure returns to its pre-compaction magnitude. Over time, if the fluid pressure does not return to its pre-compaction state, or continues to decrease, the stress on the granular skeleton causes the grains to rearrange and compact, resulting in inelastic deformation. As the volume of the aquifer affected by deformation increases, the deformation can results in permanent land subsidence.

Aquifer compaction is both a vertical and horizontal (radial) phenomenon that can manifest itself as a land surface elevation drop and/or land fissures. For instance, from 1927 to 1977, the San Joaquin valley of California experienced 9 meters of land subsidence from aquifer compaction as a result of groundwater pumping for irrigational purposes. In other areas of California and Arizona, land fissures have developed causing costly damage to homes and municipal infrastructures (Galloway et al., 1999).

The compressibility of the granular skeleton of an aquifer (compressibility is the elastic precursor to inelastic aquifer compaction) is controlled by factors such as grain size, shape and mineralogy, the amount, location and mineralogy of cementation, as well as the porosity and diagenetic history of the aquifer. Due to the variability of these factors, the solid (i.e. granular and crystalline) spans over several orders of magnitude. Even the compressibility of various sandstones can range from 10^{-10} to 10^{-8} Pa^{-1} (Wang, 2000). The effects of cementation are particularly complex because cementation affects the mechanical and hydrologic properties of the granular media by influencing both the stiffness and permeability of the granular skeleton. The first goal of this research is to quantify the effects of variable cementation on meso-scale mechanical properties of granular porous media using two dimensional Discrete Element Method (DEM) models. The DEM models allow us to investigate the effects of individual micro-scale parameters that are not directly parameterized in continuum scale models. The influence of cementation on hydrologic properties is captured by correlating the amount of cementation in the DEM models to natural samples and to the hydrologic properties of the natural samples.

The second goal is to use the results from the DEM models and corresponding hydrologic properties as input parameters into macro-scale, 2D axial symmetric poroelastic models. The poroelastic models couple fluid flow and solid deformation physics by solving the equations of poro-elasticity. By prescribing the meso-scale mechanical and hydrologic properties into the poroelastic models, we can address the implications of hydro-mechanical changes on continuum scale fluid removal and deformation.

CHAPTER 2

THE EFFECTS OF CEMENTATION ON MECHANICAL AND HYDROLOGIC PROPERTIES

The mechanical and hydrologic properties of an aquifer can vary significantly depending on how the sediment evolved during diagenesis. Diagenesis is the process of sediment undergoing physical and chemical changes, consolidation and lithification. Over time, new deposition buries previously deposited sediment, causing the underlying sediment to compact. Compaction reduces the porosity of the granular skeleton by rearranging and reshaping the grains to fill in pore space. As the sediment is buried deeper, changes in temperature and pressure induce chemical changes, such as dissolution and deposition of cementing materials (e.g. Fetter, 2001). Deposition of cementing materials such as calcite, dolomite or silica reduces the porosity and permeability of clastic material. An extensive amount of literature is dedicated to understanding the controls of porosity and permeability (Bloch, 1991; and Ahmed et al., 1991) and their relationship to one another (Kozeny, 1927; Carman, 1937, 1948, 1954; Pape et al., 2000; and Berg, 1970). Such research paved the way for investigations of the effects of cementation on permeability and porosity (Mower and Budd, 1996; Molenaar et al. 2007).

However, quantitative data on the effects of cementation on the mechanical properties of granular media is limited. Qualitative work by Dvorkin and Yin (1995) demonstrated that cement at grain contacts is load bearing and reduces elastic

deformation, suggesting that cementation increases the stiffness of the granular media. By quantifying the relationship between changes in the amount of cementation and changes in the stiffness response of granular media we constrain the relationship between granular skeleton compressibility, fluid yield and land surface deformation. The quantitative nature of this research also allows for the investigation of the competing roles of mechanical and hydrologic properties in large scale fluid flow and deformation.

CHAPTER 3

HYDRO-MECHANICS OF CONFINED AQUIFERS

The physical mechanisms that control fluid flow and deformation are different for unconfined and confined aquifers. In unconfined aquifers, the top of the aquifer is the level at which the pore water pressure is equal to atmospheric pressure, or the water table. Since the fluid in the aquifer is not pressurized, the potentiometric surface is equal to the water table. In confined aquifers, a layer of sediment with low hydraulic conductivity, known as aquitards or aquicludes, allows fluid pressure to build up in the aquifer, raising the potentiometric surface above the level of the confining unit. When fluid is pumped from a confined aquifer the pore space does not drain, as it does in an unconfined aquifer. Instead, as fluid is removed from the granular skeleton, the pore pressure drops and the effective stress on the grain skeleton increases causing the granular skeleton to contract and expel water. The remaining water in the pores expands in response to the decrease in fluid pressure and forces more water out of the granular skeleton (Ingebritsen, 2006).

Effective stress was first defined by Karl Terzaghi in 1923 to explain the behavior of saturated soil for engineering applications. Terzaghi defined effective stress as

$$\sigma_e = \sigma_{zz} - \mathrm{P}$$

where σ_{zz} is the change in external load or total vertical stress (Pa) and P is the change in the fluid pressure in the pores (Pa). For relatively small changes in effective stress, the deformation associated with the contracting grain skeleton is elastic and therefore

recoverable when the stress on the aquifer returns to its pre-stressed state. However, ground water pumping for municipal, agricultural and industrial purposes tends to significantly increase the effective stress on the granular skeleton, to the point that the granular skeleton succumbs to inelastic deformation. Inelastic deformation occurs when the stress on the grains causes the grains to shift and/or crack, resulting in permanent compaction. The compaction reduces pore volume and subsequently the potential volume of water available for fluid storage. Note that compressibility is an elastic (reversible) mechanical property of an aquifer and compaction is an inelastic (permanent) consequence of over pumping. The elastic response of an aquifer to changes in effective stress are instantaneous but inelastic compaction happens over time from continued over-pumping and can continue for years, even after pumping has ceased (Fetter, 2001).

Deformation, both elastic and inelastic, of an aquifer's granular skeleton influences fluid yield. As previously mentioned, elastic deformation (i.e. compressibility), influences fluid yield by allowing the granular skeleton to contract and expel water. The

amount of fluid absorbed or expelled from the granular skeleton per unit volume of a porous medium per unit change in head, owing to the compressibility of the granular skeleton, is referred to as the specific storage. The classic definition of one-dimensional specific storage for a confined aquifer is

$$Ss = \rho_w g(\alpha + n\beta)$$

where ρ_w is the density of water (kg m^{-3}), g is the gravitational constant (m s^{-2}), α is the compressibility of the porous media (m^2 N^{-1}), n is porosity (unitless), and β is fluid

compressibility ($m^2\ N^{-1}$). The compressibility of water (β) is approximately $4.4e^{-10}\ m^2N^{-1}$, while values for the compressibility of a granular skeleton range from 10^{-10} to $10^{-5}\ m^2\ N^{-1}$. The relatively small value of fluid compressibility compared to the compressibility of the granular media indicates that compressibility of the solid is the controlling variable of specific storage (Ingebritsen, 2006).

Early studies of specific storage by H. Jacob (1940) and C. Cooper (1966) suggested vertical deformation was far more influential on specific storage than horizontal deformation and in most cases horizontal deformation could be ignored.

Later work by Helm (1994) and Burbey (1999) determined that both the vertical and horizontal displacement components are significant for the calculation of specific storage. Burbey (1999) describes specific storage for a three-dimensional problem as

$$Ss = \rho_w g\left(\frac{3}{(3\lambda + 2G)} + n\beta\right)$$

where λ is Lame's elastic constant (Pa) and G is shear modulus (Pa). Lame's elastic constant is defined as

$$\lambda = \frac{\nu E}{[(1-2\nu)(1+\nu)]}$$

where E is Young's modulus (Pa) and ν is the drained Poisson's ratio. Young's modulus for a confined aquifer is defined as

$$E = G(2(1+\nu))$$

The expansion of the solid compressibility term (α) to individually prescribed elastic parameters (e.g. Young's modulus and Poisson's ratio) allows us to investigate the effects of changes in the amount of cementation and on the elastic response of the granular media, which directly influence the magnitude and area of deformation.

Inelastic deformation influences fluid yield by decreasing the pore volume available to store fluid. The pore volume, or porosity, also influences the compressibility of the granular skeleton. Compressibility, either granular or pore volume, refers to the ratio of a fractional volume change with respect to a pressure change. Contrary to early work by Hall (1953) who suggested that a correlation exists between low porosity rocks and pore volume compressibility, porosity alone does not seem to be a first order predictor of compressibility. Fatt (1958) suggested that Hall's correlation may have been "fortuitous" because of the samples used by Hall. Later work by Jalalh (2006) compared experimental data for pore volume compressibility and porosity of Hungarian sandstone samples as well as his own data with Hall's data and other published data. Jalalh suggests that while Hall's correlation between porosity and compressibility may exist, the correlation only works with low porosity sandstones and can not be extrapolated to higher porosity samples. Figure 1 shows the variability pore volume compressibility and porosity. In some instances (e.g. 13 percent porosity), the pore volume compressibility ranges over two orders of magnitude for a single value of porosity (Jalalh, 2006). We suggest that some of the variability observed in the values of compressibility can be accounted for by a quantitative understanding of the effects of cementation at the grain scale.

Such an understanding also provides the opportunity to better predict fluid yields as well. Figure 1 depicts the correlation between porosity, pore volume compressibility and fluid yield as the porosity and pore volume compressibility were used to calculate the fluid yield on the right axis. The strong relationship is controlled by both the pore volume compressibility and the porosity. However, the extent to which cementation affects each

is unclear. Therefore, a quantitative understanding of the effects of the cementation on pore volume compressibility will help refine calculations of fluid yield.

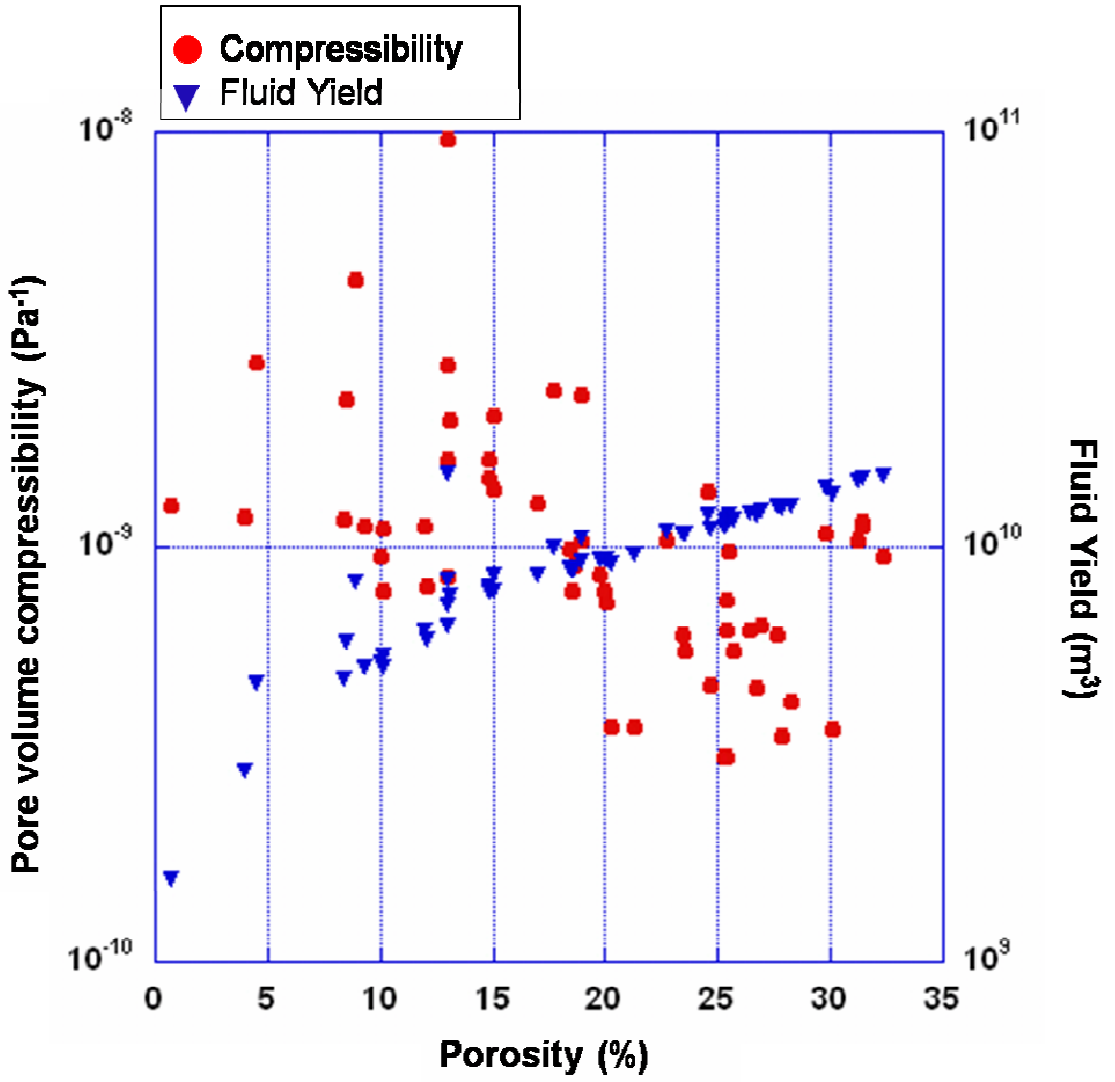

Figure 1. The left axis is pore volume compressibility plotted against porosity for a variety of sandstone samples.The right axis is the calculated fluid yield for the corresponding porosities and pore volume compressibility for 50 meters of drawdown. Recreated from Jalalh (2006).

CHAPTER 4

DEM MODELS AND THE ROLE OF CEMENTATION ON MECHANICAL PROPERTIES

4.1 Discrete Element Method

DEM models are utilized in this research because they have been demonstrated to be a robust tool for simulating the interactions between grains and allow the prescription of individual parameters that are otherwise lumped in continuum models. The discrete element method used in this work, is a solid mechanic technique first described by Cundall (1971) and Cundall and Strack (1979). This technique has successfully approximated the behavior of noncohesive, granular systems under low stress conditions (Cundall et al., 1982; Cleary and Campbell, 1993; Campbell et al., 1995; Morgan, 1999; Morgan and Boettcher, 1999) and lithified sedimentary rocks (Bruno and Nelson, 1991; Potyondy et al., 1996; Hazzard et al., 2000; Boutt and McPherson, 2002).

In this paper, we use a traditional DEM approach that shares many similarities to those presented by Cleary and Campell (1993); Campbell et al. (1995); Morgan (1999); Morgan and Boettcher (1999), that is ultimately based on an existing two-dimensional DEM application (Rege, 1996; Williams and Rege, 1997). The DEM code used in this paper is identical to the lattice-Boltzmann DEM (LBDEM) code described by Boutt et al. (2007). Although the LBDEM code is capable of solving coupled fluid-solid problems, this work focuses only on the solid-solid interactions.

DEM models simulate the mechanical behavior of porous media by idealizing the system as a collection of separate grains that interact at their contact points (Figure 2). Within the DEM models, grains are assumed to be rigid, with grain deformation occurring only at contact points (Cook et al., 2004). The method identifies the grains in contact and then resolves the contact physics by alternating between the application of Newton's Second Law and a force-displacement law. The force-displacement law relates components of force to corresponding components of relative displacements through a generalized contact constitutive model. The applied contact constitutive model is comprised of a stiffness model and a slip model. The motion equations are integrated explicitly with respect to time to obtain grain positions. The positions at each time step are used in force-displacement calculations and the calculation cycle starts over again (Boutt et al., 2007). Force-displacement should not be confused with stress-strain. Stresses are assigned to the confining platens during the simulations while the force-displacement is a result of the stiffness of the models. The basic theory of DEM and its methods is given by Pande et al. (1990).

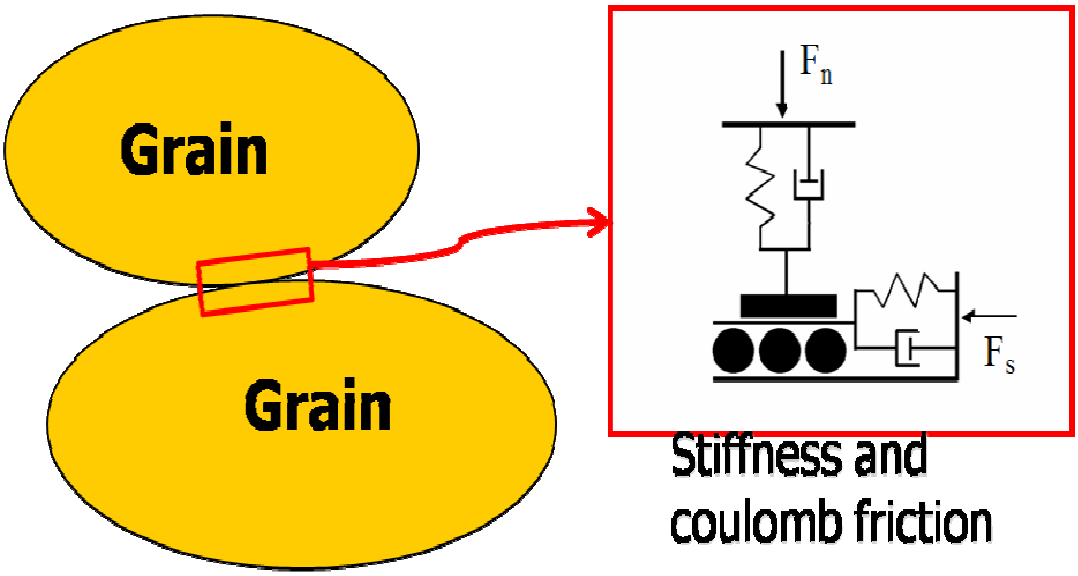

Figure 2. Schematic diagram of the interaction between two grains. The grains are kept from rotating by the stiffness of the grains and coulomb friction.

4.2 The Bonding Scheme

A bonding scheme was applied to the grains in order to simulate the behavior of a cohesive rock. Neighboring grains were bonded together by point to point constraints using the spring formulation as

$$F_b = k_b \Delta x$$

where F_b is the force on the bond (N), k_b is the bond stiffness (N m^{-1}), and Δx is relative displacement of the neighboring particles (m). The bonds are aligned with the surface normals and connect the closest centroids of two adjacent particles. If F_b is greater than or equal to the bond strength (F_b^{crit}) the constraint is removed and bonded grains are allowed to move freely. This bonding approach has no implicit shear strength. In reality, the bond has some finite shear strength since it is modeled as a surface to surface contact and any offset (normal or tangential) great enough to exceed the F_b^{crit} will cause the bond to fail (Boutt et al., 2007). A schematic of two force-displacement curves is shown in Figure 3.

The number of bonds in the model is controlled by the bond radius. The bond radius is the distance between the centroids of two grains. When a bond radius is prescribed all the neighboring grains with centriods within the prescribed radius are bonded. The bond radius is limited by the smallest grain radius in order to keep the bonds from forming across grains that are not adjacent to each other. By varying the bond radius we can control the number of bonded grains in the simulations.

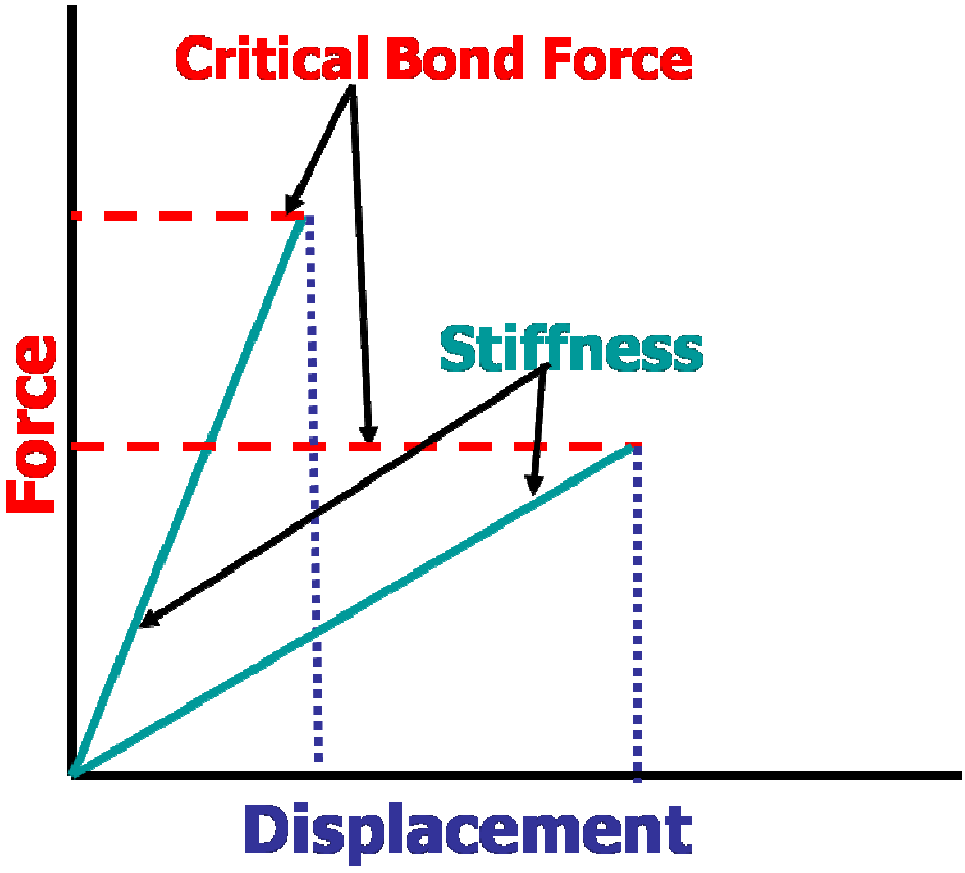

Figure 3. Schematic diagram of the effects of bond stiffness on the force-displacement curve.

4.3 DEM Models

The 2D biaxial models are designed to replicate laboratory triaxial tests (Figure 4). Triaxial tests are generally preformed on natural rock cores in order to determine the mechanical properties (e.g. Young's modulus and Poisson's ratio) of the samples. The same objective can be accomplished with 2D biaxial tests of DEM models.

The biaxial test apparatus is built by first creating a test vessel with rigid platens. The size and shape of the grains are defined (grain size can be defined as a diameter range of an equal distribution and grain shape and can be uniform or mixed). The grains are then deposited into the test vessel and consolidated under gravity. Once the grains are consolidated, a confining stress of 0.2 N m^{-1} is applied to both the confining quads and platens, until the forces on the platens come to equilibrium. The model is considered to be at equilibrium when all the contact force vectors on the grains are approximately equal. The model is saved in this state of equilibrium, without any grain to grain bonds. This process is repeated for each grain geometry (ellipsoidal, circular and mixed). The bonds are prescribed before the start of each simulation and the confining stress on the platens is then changed to a constant velocity of 0.01 m sec^{-1}. The stress on the confining quads remains the same throughout the entirety of the model preparation and simulation.

In order to test the mechanical properties of a sample (natural samples or modeled), the test is run until the sample fails. In numerical and laboratory tests inelastic deformation is expressed as non-linearities on stress-strain curves. The change in slope indicates grain re-arrangement and/or breakage. For simulations that do not produce the classic linear stress/strain curve, snap shot images of the model during the simulation are

used to identify shear bands that also signify inelastic behavior. Shear bands signify inelastic behavior because grains have rearranged in order to form the bands.

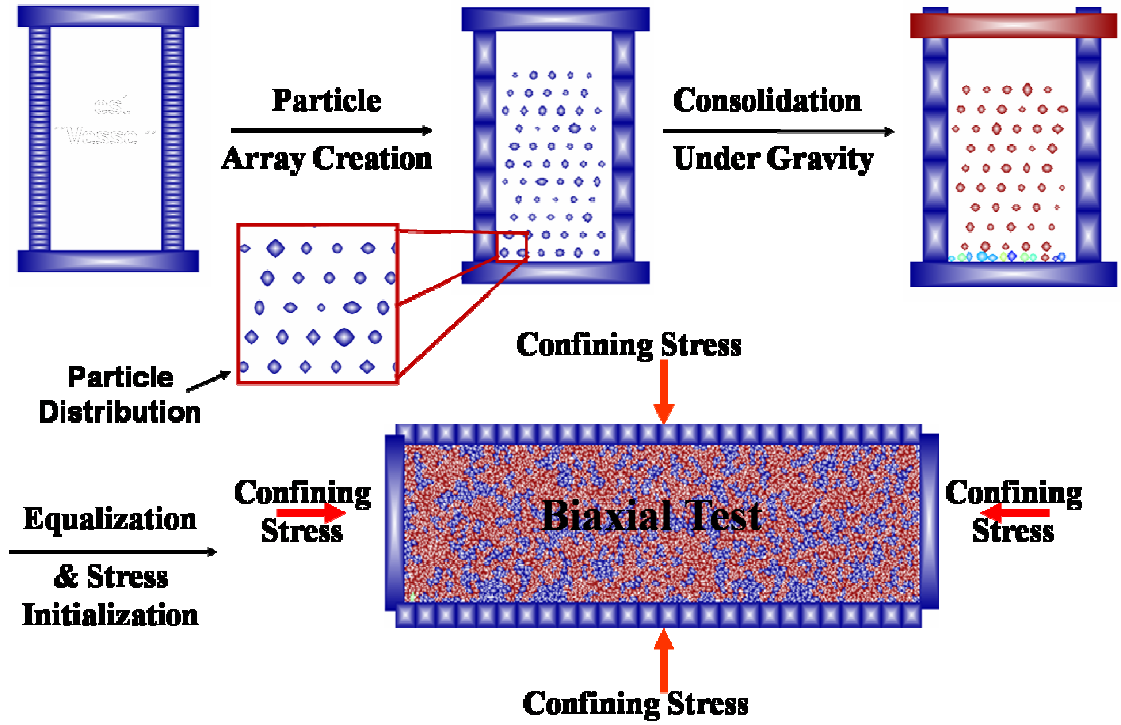

Figure 4. Typical DEM model creation process and conceptual model.

4.4 DEM Parameters

The numerous parameters in the DEM models allow for control and versatility in prescribing individual parameters such as the stiffness of bonds, grains and platens as well as parameters such as gravity.

Bond stiffness controls the amount of displacement the bond can withstand before failure. The bond stiffness can be changed to reflect different cement mineralogies. For this study, the material properties of the bonds and grains are scaled to be analogous to the properties of quartz. The grain properties are similar to those presented in Boutt et al., (2007). A full list of the values for DEM parameters are in Table 1.

The platen stiffness is set at a value high enough as to not allow deformation of platens. The high value of stiffness of the platens insures that all the displacement recorded is displacement from the compression of the grain skeleton and not deformation of the platens. The interaction between the confining quads, platens and grains are controlled by assigning material values that are dependent on which material they are contacting. For example, the assigned stiffness of a platen at the point where the platen is in contact with a grain is 100 N m^{-1} but points of contact between the confining quads and the platens have a stiffness of $1x10^{-6}$ N m^{-1} By adjusting the stiffnesses accordingly, the platens and confining quads are allowed to slide past each other during the simulation but still be competent against the grains.

The friction between grains is set to simulate friction in natural systems (Boutt et al., 2007). Setting the friction in this manner keeps the grains from slipping past each other unrealistically.

Gravity is turned on and off at different times during the model preparation and simulation. During the model preparation gravity is used to consolidate the grains but is turned off again before the start of the simulation. Gravity is not considered in these models because the influence of gravity is insignificant compared to the other forces in the model.

Table 1. Parameters of the DEM models

Parameter	**Value**
Friction, dimensionless	0.8
Grain normal stiffness, N m^{-1}	1.0
Grain shear stiffness, N m^{-1}	0.6
Bond strength, N	0.01
Bond stiffness, N m^{-1}	200
Mean Grain Diameter, m	0.018
Platen Velocity, m s^{-1}	0.01
Confining stress, N m^{-1}	0.2^{1}
Timesteps, sec	$6x10^{-5}$
Dimensions, m	0.035 x 0.132

4.5 Quantifying the bonds

Since the bonds are modeled as simple point to point constraints, the thickness of the bonds is negligible and we cannot use the area of the bonds to quantify the cementation in the models. Therefore, instead of using the area of the bonds we have developed a bond to grain ratio (BGR) for each model. The BGR is the number of bonds in the model divided by the total number of grains. The BGR is used to quantify the amount of cement in the models as well as correlate the models to natural samples. The correlation between the BGR in the DEM models and the BGR of natural samples is discussed in section 6.

CHAPTER 5

DEM RESULTS

The DEM models were designed to elucidate the effects of increased cementation and grain packing (identified by grain geometry) on bulk elastic and inelastic parameters. The results reported in this section are for the ellipsoidal grains; the results for the circular and mixed grain geometries are in the appendix. Figure 5 is a time series of the BGR 1.00 model simulation. Snapshot 5a is the original dimensions of the model at the start of the simulation. Progression through snapshots 5b and 5c show that over time the models respond elastically to the compression applied at the left and right boundaries by shortening and barreling. Snapshot 5c also shows the beginning of inelastic failure in the form of a fracture near the bottom center of the image. In snapshot 5d the model has inelastically failed, as signaled by the fractures in the image. From these simulations, we record the changes in the axial and lateral dimensions of the models with increased force. The changes in stress and strain are calculated by tracking changes in the force and displacement of the platens and confining quads. The slope of the stress-strain data for each BGR simulation provides a value of Young's Modulus for each model (Figures 6). The increasing values of Young's Modulus from BGR .5 to BGR 2.25 indicate the model stiffens with increased cementation (Figure 7).

Contrastingly, as Young's Modulus increases, Poisson's ratio decreases because the stiffening of the granular skeleton resists deformation from changes in stress. In order

to calculate Poisson's ratio for a two dimensional model the following equation is used to account for the plane stress and plane strain assumptions.

$$\nu_{pstrain} = \frac{\nu_{pstress}}{1 - \nu_{pstress}}$$

where

$$\nu_{pstress} = \frac{\varepsilon_L}{\varepsilon_A}$$

and ε_L is the lateral strain and ε_A is the axial strain on the model. ε_L and ε_A are defined as

$$\varepsilon_L = \frac{W_f - W_i}{W_i}$$

$$\varepsilon_A = \frac{L_i - L_f}{L_i}$$

where W_f, W_i, L_i, L_f is the final width, initial width, initial length and final length of the models, respectively (PFC^{2D}, 1999). The resulting values of Poisson's ratio from the DEM models are listed in Table 2.

In order to simplify reporting the results, the changes in the elastic response have been calculated as a change in shear modulus. The relationship between Young's Modulus, Poisson's ratio and shear modulus is defined as

$$G = \frac{0.5\mathrm{E}}{1 + \nu}$$

where E is Young's modulus (Pa) and ν is Poisson's ratio (Wang, 2000). Decreasing the BGR from 2.25 to 0.5 resulted in a five fold decrease in shear modulus (Table 2). In order

to scale the elastic DEM model results up to a macro-scale investigation, the shear modulus calculated for each BGR was used as an input parameter for individual aquifer scale poroelastic models.

Although the main focus of the DEM models is the elastic response of the models, inelastic changes were observed and recorded too. The increased stiffness of the models from increased cementation allows the models to withstand higher stresses and produce less strain before failure even though the critical bond force is the same in each model (Figure 6). The inelastic results (yield strengths) are listed in Table 2.

Changes in the amount of cementation also change the deformation patterns at the final timesteps of the models (Figure 8). At BGR of 0.5 the amount of cementation is so minute that displacement is accommodated by multiple sets of shear bands forming in areas of low cementation. As the amount of cementation increases the deformation becomes more focused and forms only a single shear band, suggesting that deformation is localized in the high cementation simulations.

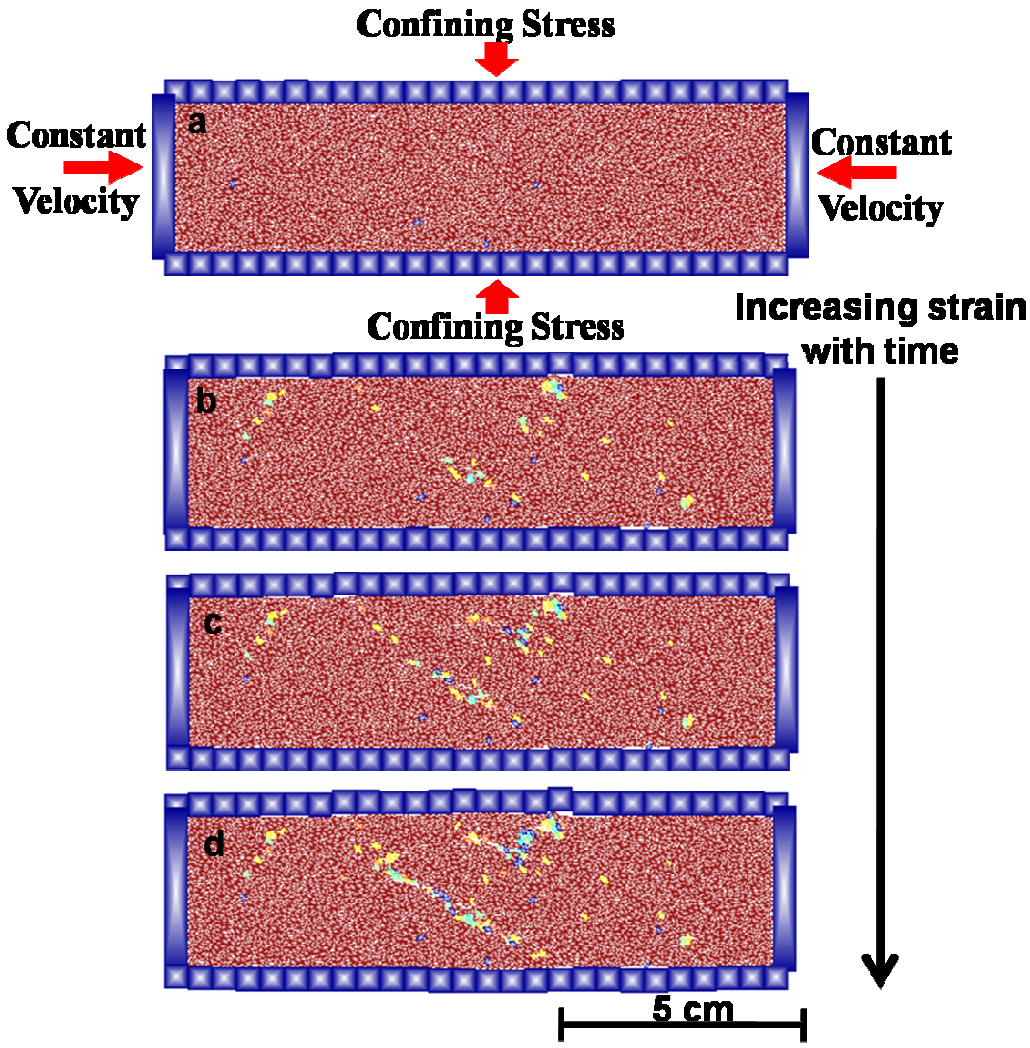

Figure 5. Time series of a DEM model.

Table 2. The elastic and inelastic results for the ellipsoidal grain simulation as a function of BGR.

BGR	Young's Modulus (Pa)	Poisson's Ratio	Shear Modulus (Pa)	Yield Strength (Pa)
0.5	2.6×10^{8}	0.56	8.9×10^{7}	2.1×10^{6}
1.00	6.9×10^{8}	0.48	2.4×10^{8}	1.0×10^{7}
1.85	9.3×10^{8}	0.28	3.6×10^{8}	1.5×10^{7}
2.25	1.2×10^{9}	0.27	4.8×10^{8}	1.6×10^{7}

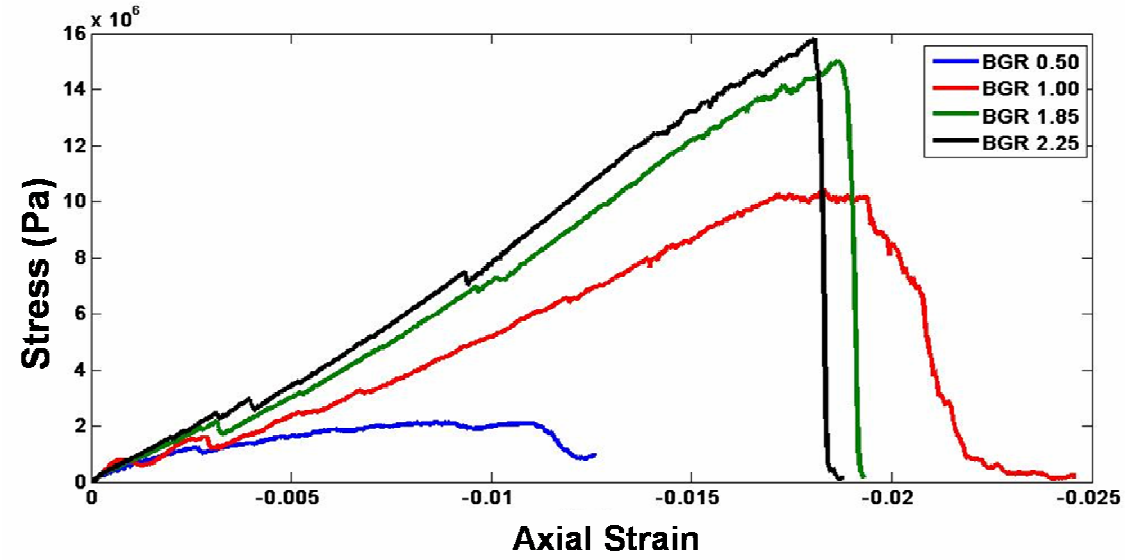

Figure 6. Stress-strain plots for each BGR.

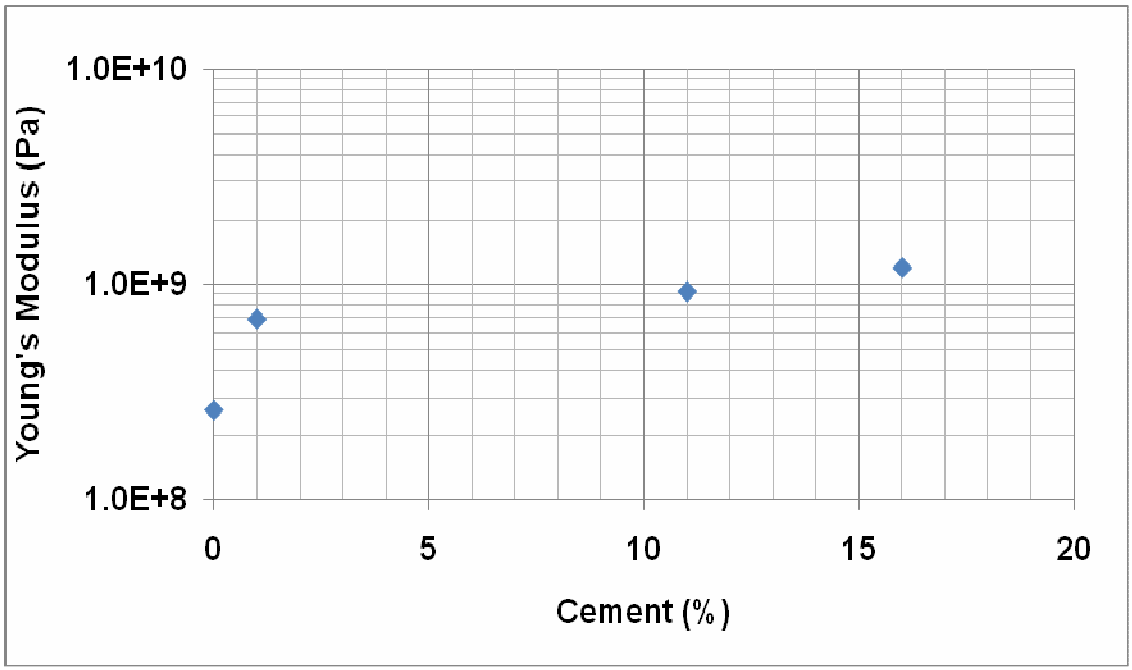

Figure 7. Young's modulus as a function of increasing percent cementation.

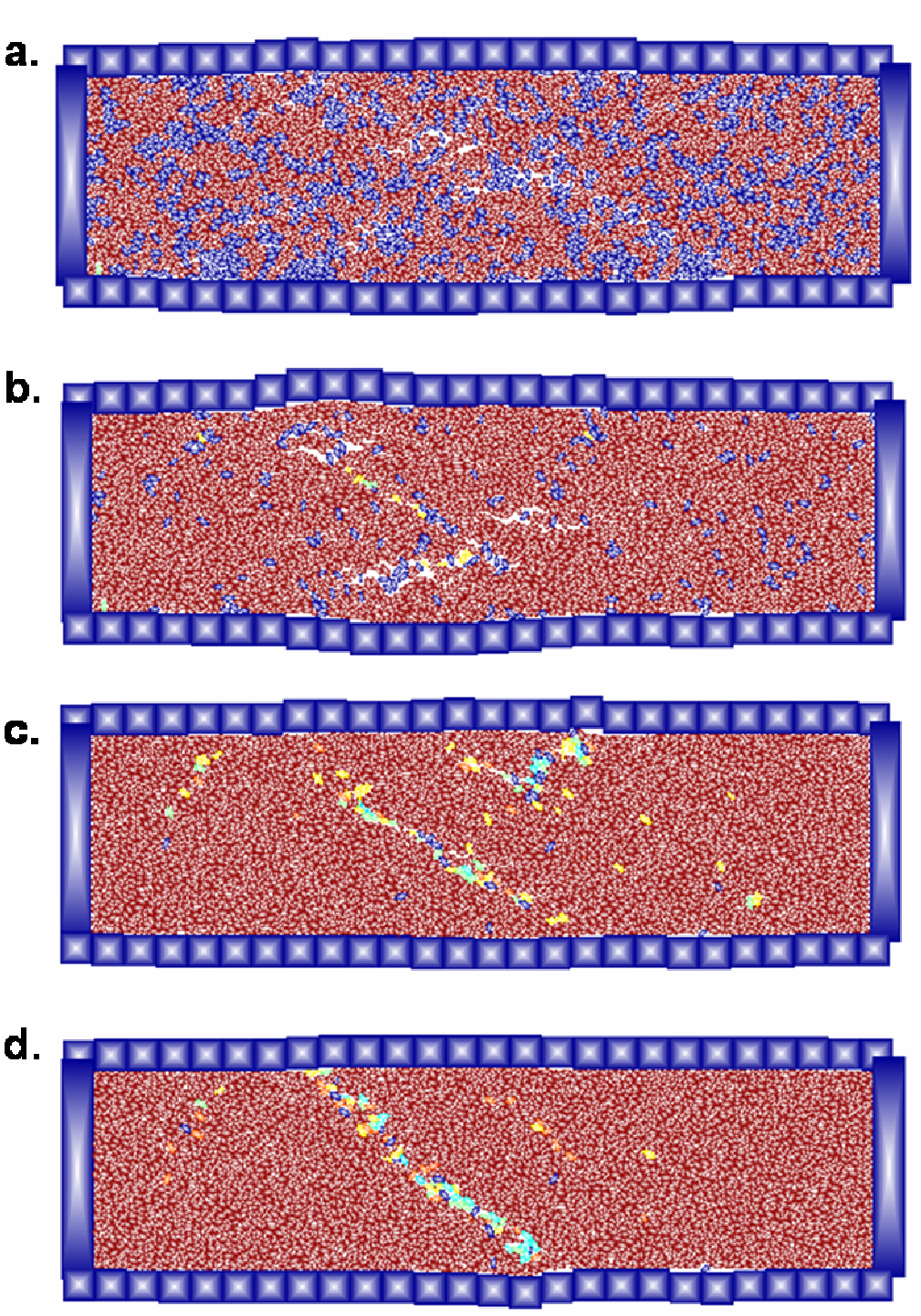

Figure 8. Inelastic deformation patterns at the end of each DEM model for BGR 0.5 (a), 1.0 (b), 1.85 (c), and 2.25 (d).

CHAPTER 6

CORRELATING THE DEM BONDS TO NATURAL SAMPLES

The St. Peter sandstone is the natural analog for the DEM models. The St. Peter sandstone is a quartz arenite with variable quartz cement. The hydromechanical properties (percent cement, porosity and permeability) of five samples of the St. Peter sandstone were characterized. For each sample, a composite of 25 cathodulminescence images were used to count the grains and grain bridging cement contacts (Figure 9). The number of grain bridging contacts was divided by the number of grains to determine the natural samples' BGR. Once the BGR was established for each natural sample, the BGR and percent cement was plotted and a line was fit to the data (Figure 10). After fitting a line to the data, we determined the corresponding percent cement for each BGR used in the DEM models. The percent cementation for each natural sample was calculated from a point count of the cathodulminescence images used to determine the BGRs. The area of the cement, grains and pore space are dipicted in Figure 9.

The relationships between the percent cement, porosity and permeability of the natural samples were graphed and used to determine values of porosity and permeabilibty for the poroelastic models (Figure 10). The porosity of the St. Peter sandstone was calculated using a helium pycnometer. The helium pycnometer measures the volume and true density of solid objects by calculating the amount of helium that is displaced into the pores of the solid. The permeability of the natural samples is measured using a tinyperm

permeameter. The tinyperm permeameter has a rubber nozzle attached to a syringe that is pressed against the rock sample. Using the syringe, air is withdrawn from the rock sample and as the air is pulled from the sample, a micro-controller unit simultaneously monitors the syringe volume and the transient vacuum pulse created at the sample surface. The tinyperm then uses signal processing algorithms to compute the response function of the sample/instrument system to provide a value of permeability for the sample (New England Research, 2008). By correlating the DEM models to the natural samples, we are able to quantify the amount of cement in the models as well as investigate the importance of the influence of mechanical and hydrologic properties.

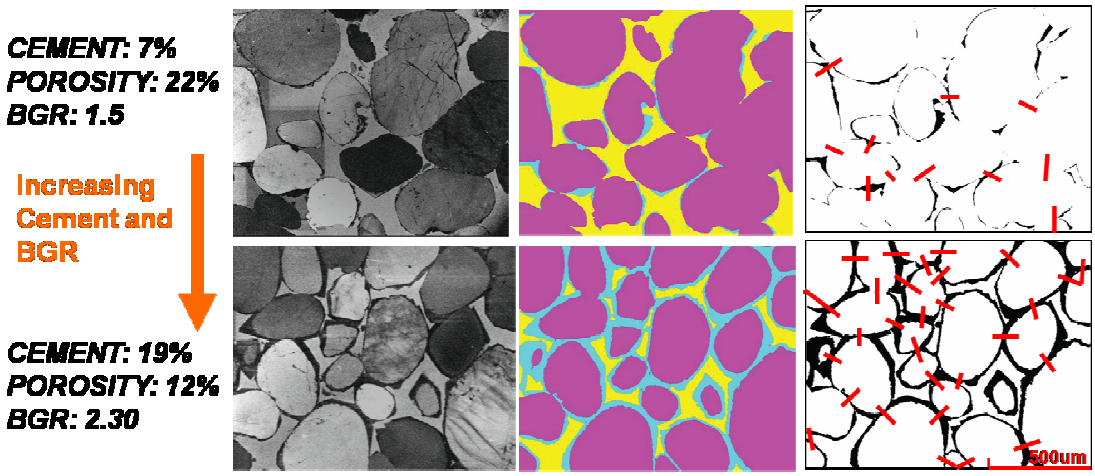

Figure 9. Cathodulminescence images of the St. Peter sandstone. From left to right : Column 1) Unaltered cathodoluminescence images. Column 2) The same thin section images with alterations to show the grains as purple, cement as blue and pore space as yellow. Column 3) Visualization of only the cement. The red lines highlight grain bridging cement. Images courtesy of Jennie Cook at the University of Wisconsin, Madison.

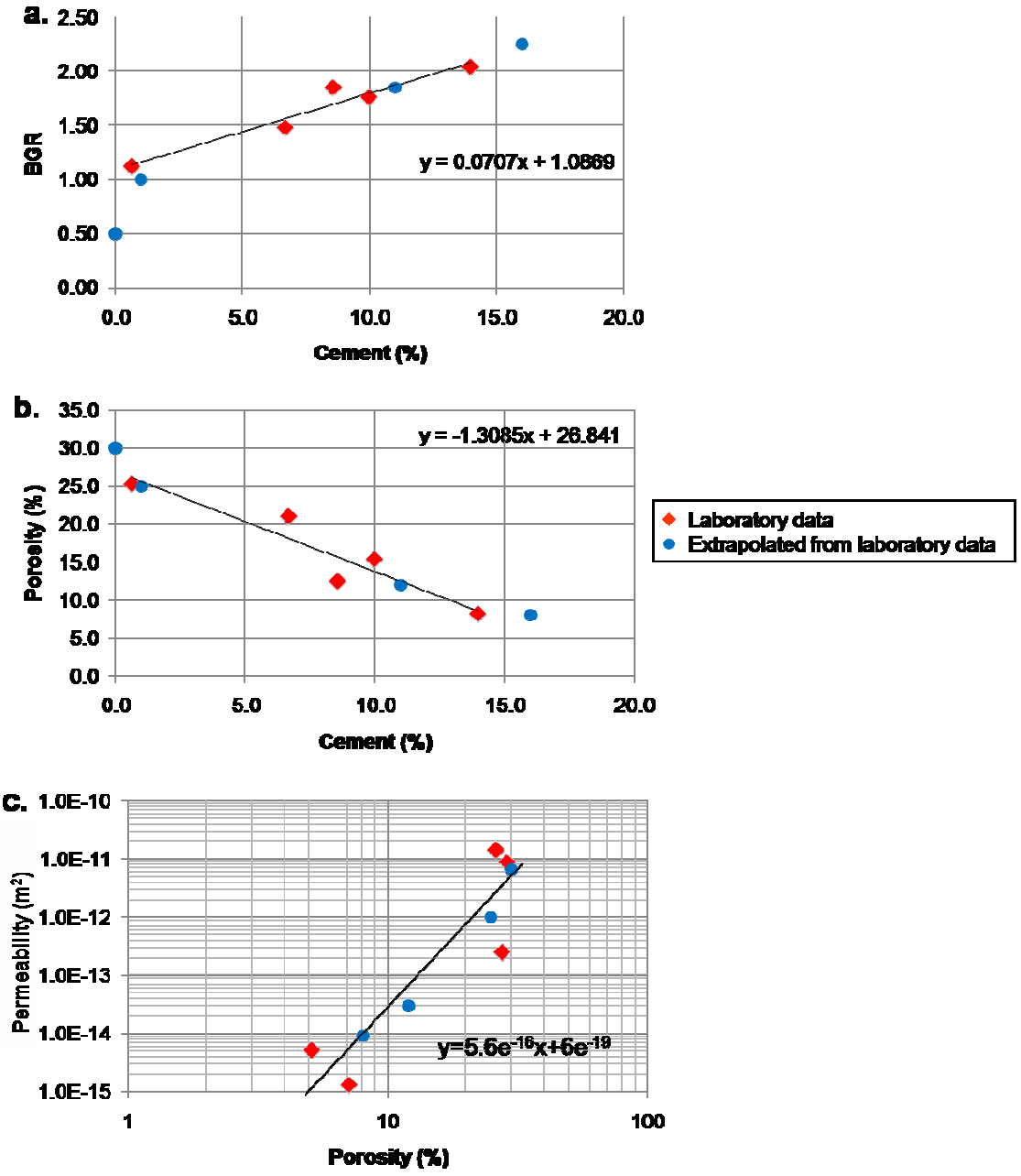

Figure 10. The measured hydrologic properties of the St. Peter sandstone and the corresponding calculated properties for the DEM and poroelastic models plotted as **a)** percent cement versus BGR, **b)** Percent cement versus porosity and **c)** porosity versus permeability.

CHAPTER 7

POROELASTIC MODELING APPROACH

Two dimensional, axial symmetric, poroelastic models were used investigate the effects of micro-scale mechanical and hydrologic properties on aquifer-scale fluid flow and deformation. This research utilized Comsol Multiphysics, a finite element method code designed to solve the equations of linear poroelasticity and provide transient fluid-solid deformation solutions. Two linear constitutive equations form the framework for Biot's 1941 theory of poroelasticity for an elastic, isotropic, fluid-filled porous medium. The equations are defined as follows:

$$\varepsilon = a_{11}\sigma + a_{12}p$$

$$\zeta = a_{21}\sigma + a_{22}p$$

The equations state that a change in applied stress (σ) and fluid pressure (p) produce both a fractional volume change (□) of the media, which results in fluid being added to or removed from storage (ζ). The variable a is generic coefficient (Wang 2000). The relationship between changes in stress-strain and fluid storage is the basis for the fluid-solid coupling in Comsol, as provided by the Darcy's Law application in the Earth Science module and the axial symmetry, stress–strain application in the Structure Mechanics module. For an axisymmetric problem, with pressure as the fluid-coupling variable, the displacement equations for the vertical and radial directions are

$$G\left(\frac{\partial^2 u_z}{\partial r^2}+\frac{1}{r}\frac{\partial u_z}{\partial r^2}+\frac{\partial^2 u_z}{\partial z^2}\right)+\frac{G}{1-2\nu}\frac{\partial \varepsilon}{\partial z}-\alpha\frac{\partial p}{\partial z}=0$$

$$G\left(\frac{\partial^2 u_r}{\partial r^2}+\frac{1}{r}\frac{\partial u_r}{\partial r}-\frac{u_r}{r^2}+\frac{\partial^2 u_r}{\partial z^2}\right)+\frac{G}{1-2\nu}\frac{\partial \varepsilon}{\partial r}-\alpha\frac{\partial p}{\partial r}=0$$

where G is shear modulus (Pa), u is a component of displacement, r and z are cylindrical coordinates (m), ν is Poisson's ratio, □ is volumetric strain (dimensionless) and α is the Biot-Willis coefficient (dimensionless). The axisymmetric fluid continuity equation is defined as

$$\frac{k}{\mu}\left(\frac{\partial^2 p}{\partial r^r}+\frac{1}{r}\frac{\partial p}{\partial r}+\frac{\partial^2 p}{\partial z^2}\right)-\alpha\frac{\partial \varepsilon}{\partial t}=S_\varepsilon\frac{\partial p}{\partial t}$$

where k is permeability (m^2), μ viscosity (Pa s) and $S_{□}$ (m^{-1}) is the constrained specific storage. Since p is defined by

$$p=\rho g h$$

where ρ is the density of the fluid (kg m^{-3}), g is acceleration due to gravity (m s^{-2})and h is the hydraulic head (m), p can be substituted for

$$h=\frac{p}{\rho g}$$

(Wang 2000).

The feedback between the fluid (changes in fluid pressure) and the solid (changes in displacement) result in a fluid-to-solid and solid-to-fluid coupling. The fluid-to-solid coupling occurs when a change in fluid pressure or fluid mass produces a change in the volume of the granular skeleton. Likewise, the solid-to-fluid coupling happens when a change in applied stress produces a change in fluid pressure of fluid mass (Wang, 2000).

The models are solved iteratively, allowing for the changes in stress and strain to be calculated at each time step. The model details are listed in Table 3. (Comsol, 2006)

Table 3. Details of the poroelastic models.

Model Properties	
Analysis type	transient
Linear system solver	direct (UMFPACK)
Time dependent solver	0:1:8640000
Timesteps	free
Relative tolerance	0.01
Absolute tolerance	0.001

7.1 Conceptual Model

The conceptual model for the poroelastic models is a cylindrical confined aquifer 100 meters thick and 160 kilometers in diameter (Figure 11). The initial hydraulic head throughout the domain is specified at 200 meters. A fully penetrating pumping well draws the fluid down and holds the fluid level at a constant head of 150 meters at the pumping well. This boundary condition of specified head was chosen in lieu of a specified flux (i.e. pumping rate) to explore the transients that develop in models with drastically different hydraulic conductivities. This approach enables us to observe changes in the progression of dewatering and deformation from the pumping well, across the aquifer as a result of the changes in hydraulic conductivities. All the remaining hydraulic boundary conditions are zero flux (or no flow / impermeable boundaries). For the mechanical boundary conditions, the displacement boundary condition at the well is zero radial displacement and zero vertical stress. All the other boundaries are allowed to displace in the radial and vertical directions, except the bottom boundary which has no vertical displacement. The input parameters are listed in Table 4.

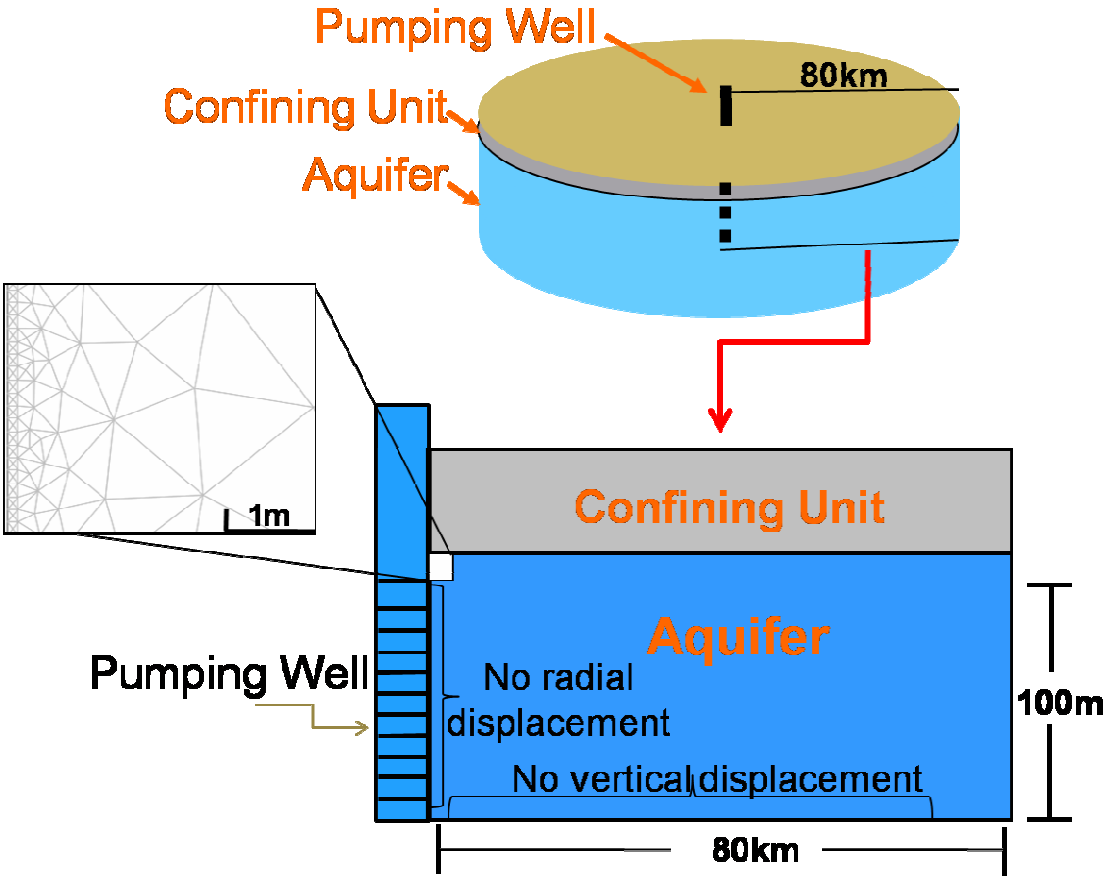

Figure 11. Boundary conditions and mesh for the poroelastic models. The aquifer is isotropic, fully confined and completely penetrated by a pumping well. The far right boundary is allowed to displace vertically and radially. The box on the left shows the mesh near the well.

Table 4. The constant input parameters used in the poroelastic models.

Constants	**Value**	**Definition**
b	100	thickness of the aquifer (m)
r_w	0.05	radius of well (m)
α	1	Biot-Willis Coefficient
ρ_f	1000	density of pore fluid (kg/m^3)
ρ_s	2200	density of solid grains (kg/m^3)
β	4.40E-10	fluid compressibility ($m^2\ N^{-1}$)

7.2 2D Axial Symmetric Poroelastic Models

As discussed in section 5, the constitutive behaviors from the DEM models, were used to calculate elastic mechanical properties (shear moduli) as a function of percent cement and then used as input parameters for the poroelastic models. Three sets of poroelastic models (nine models in total) were used to evaluate the influence of elastic mechanical (shear modulus) and hydrologic (porosity and permeability) properties on fluid flow and deformation. The goal of the first set of models was to investigate the influence of changes in shear modulus on fluid flow and deformation. One model was run for each BGR, with the corresponding value of shear modulus. The same permeability was used for all three simulations (Table 5).

The goal of the second set of simulations was to evaluate the importance of including the hydrologic properties specific to each BGR (Table 5). These three models use the same mechanical properties for each BGR as the previous set of models but this time the hydrologic properties were assigned to the specific BGRs as described in section 4.5.

The third set of models incorporated the specific values of both the mechanical and hydrologic properties for each BGR. By setting up the three sets of models in this fashion we can address the changes in fluid flow and deformation associated with changes in only elastic mechanical properties and only the hydrologic properties and compare those results to the changes associated with variations in both elastic mechanical and hydrologic properties.

Table 5. The elastic mechanical and hydrologic properties used in the poroelastic models. See Figure 10.

BGR	Altered Properties	Shear Modulus (Pa)	Permeability (m^2)	Porosity (%)
1.00				
	Mechanical	$7x10^8$	$1x10^{-13}$	15
	Hydrologic	$9x10^8$	$1x10^{-12}$	25
	Mech. & Hydro.	$7x10^8$	$1x10^{-12}$	25
1.85				
	Mechanical	$9x10^8$	$1x10^{-13}$	15
	Hydrologic	$9x10^8$	$3x10^{-14}$	12
	Mech. & Hydro.	$9x10^8$	$3.x10^{-14}$	12
2.25				
	Mechanical	$1x10^9$	$1x10^{-13}$	15
	Hydrologic	$9x10^8$	$9x10^{-15}$	8
	Mech. & Hydro.	$1x10^9$	$9x10^{-15}$	8

CHAPTER 8

POROELASTIC RESULTS

For each simulation the deformation at 1, 10 and 100 days and the change in the deformation pattern for both vertical and horizontal deformation was recorded. The raw data is listed in Appendix B. The results from all nine models are plotted to show the magnitude of vertical and radial displacement as a function of the distance from the pumped well (e.g. Figure 12). Vertical displacement is greatest near the well and lessens away from the well. The dots on the x and y-axis in Figure 12a highlight the magnitudes of maximum deformation and the distances from the pumped well at which the vertical deformation is the zero at 1, 10, and 100 days. Figure 12a shows that over time, the area influenced by vertical deformation increases in response to changes in fluid pressure which form a cone of depression around the well (Figure 13). Figure 14 is a series of snapshots of the aquifer near the pumping well for both vertical (Figure 14 a, b and c) and radial deformation (Figure 14 d, e and f) at 1, 10 and 100 days. The images are zoomed into the area directly adjacent the pumping well in order to demonstrate the deformation caused by the prorogation of the cone of depression migrating from the pumping well. This trend is consistent for all simulations.

The trend of radial deformation is different from the vertical deformation in that the location of maximum deformation is not next to the pumped well but at some distance from the pumped well (Figure 12b). The region of maximum radial displacement gets

further from the pumped well as the area affected by radial deformation increases. As with Figure 12a, the magnitudes of maximum deformation and the corresponding distance from the pumped well at 1, 10, and 100 days is marked by colored dots. Figure 15 presents a composite of all the locations of the minimum and maximum displacements and magnitudes of deformation for the vertical and radial deformation.

All the models show an increase in deformation and drawdown over the course of the 100 day simulations and a decrease in the magnitude of deformation with increased BGR (Figure 15). The decrease in deformation with increasing BGR (percent cement) reflects the stiffening response of the granular porous media with increasing cement observed in the DEM models. Beyond these initial trends, the magnitude and area of deformation varies with mechanical and hydrologic properties. In the first set of models, only the shear modulus was changed for each simulation (Figure 15a and b). Although the magnitude of deformation for each model varies somewhat, the range of values is less than that of the models that included variations in hydrologic properties (Figure 15c, d, e and f).The comparison of Figure 15a and b to Figure 15c, d, e and f suggests that the hydrologic properties significantly control the magnitude and location of deformation. This is a reasonable result considering that the hydrologic properties control the fluid flow and the fluid withdrawal is the cause of the deformation. In the first set of models where only the shear modulus changes with BGR, the hydrologic properties are set relatively high as to isolate the effects of changes in shear modulus and not restrict the deformation because of restricted fluid flow (Table 4).

For the second set of models, where only the hydrologic properties were changed with each BGR, the models produced a wider range of magnitudes and areas influenced

by deformation was observed than in the first set of models. The increased variation in results suggests that the models are more sensitive to the changes in hydrologic properties than mechanical properties.

The third set of models, included corresponding mechanical and hydrologic properties as determined by the BGRs and properties of the natural samples. Varying both the mechanical and hydrologic properties resulted in slightly higher values of vertical and radial deformation for BGR 1.00 but lower values for BGR 2.25. This set of models captures the end member behavior of both the magnitude and area of deformation not represented in typical continuum scale models.

In summary, the models that did not include changes in both the mechanical and hydrologic properties with changing cementation did not fully estimate deformation. For the most realistic case of including the changes in mechanical and hydrologic properties associated with changes in cementation, the decrease in BGR from 2.25 to 1.00 resulted in a 1.4 and 11 fold increase in vertical and radial deformation respectively.

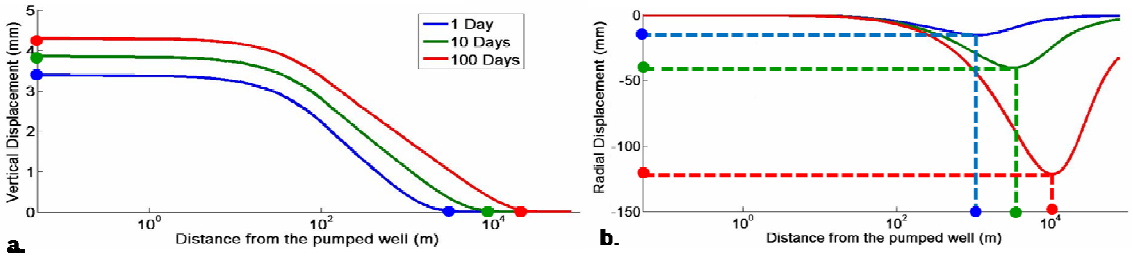

Figure 12. Plots of the magnitude and distance from the pumped well of surface deformation. The dots highlight the distance from the pumped well at which the maximum displacement occurs for each prescribed time and the value of maximum displacement. **a)** Vertical and **b)** radial deformation from a poroelastic model showing the points plotted in Figure 15.

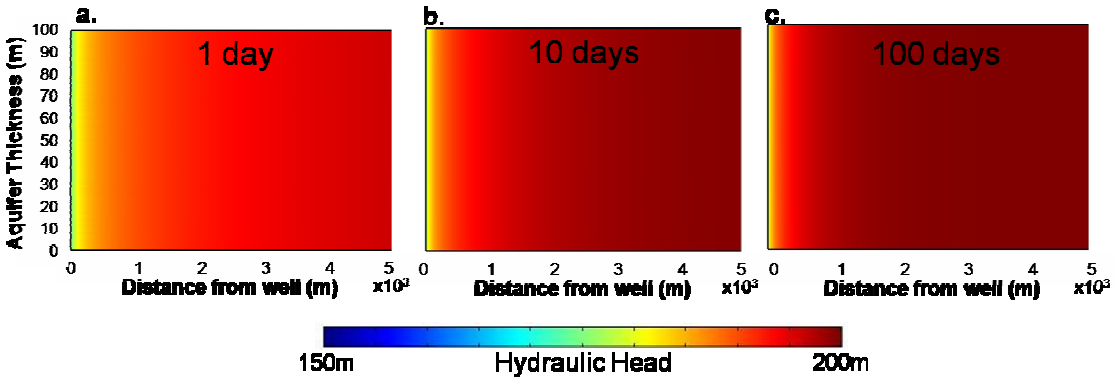

Figure 13. Spatial distribution of hydraulic head at 1, 10 and 100 days.

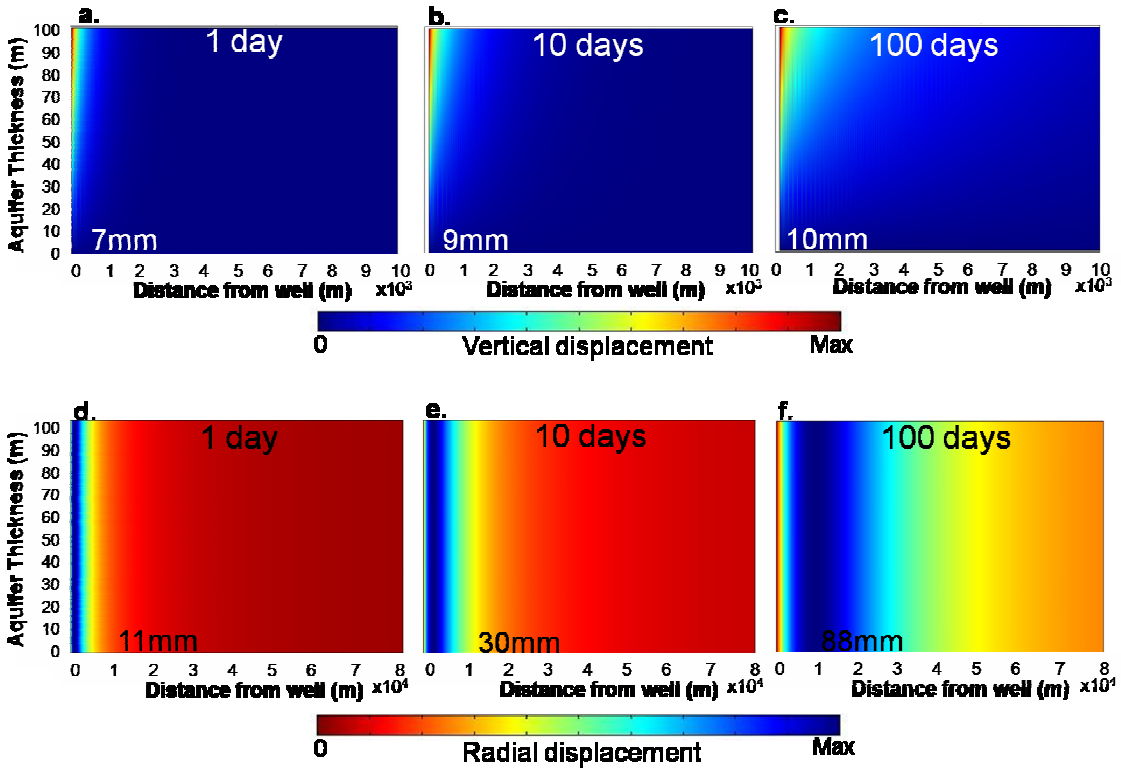

Figure 14. Snapshots of vertical and radial deformation near the pumping well after **a** and **d)** 1, **b** and **e)** 10 and **c** and **f)** 100 days of pumping, respectively. The snapshots of vertical displacement are zoomed into the region near the pumped well (the pumped well is on the left) to show the entire thickness of the aquifer but only extend 10 km horizontally. The snapshots of radial displacement are the set up the same as the vertical displacement except they extend 80 km horizontally.

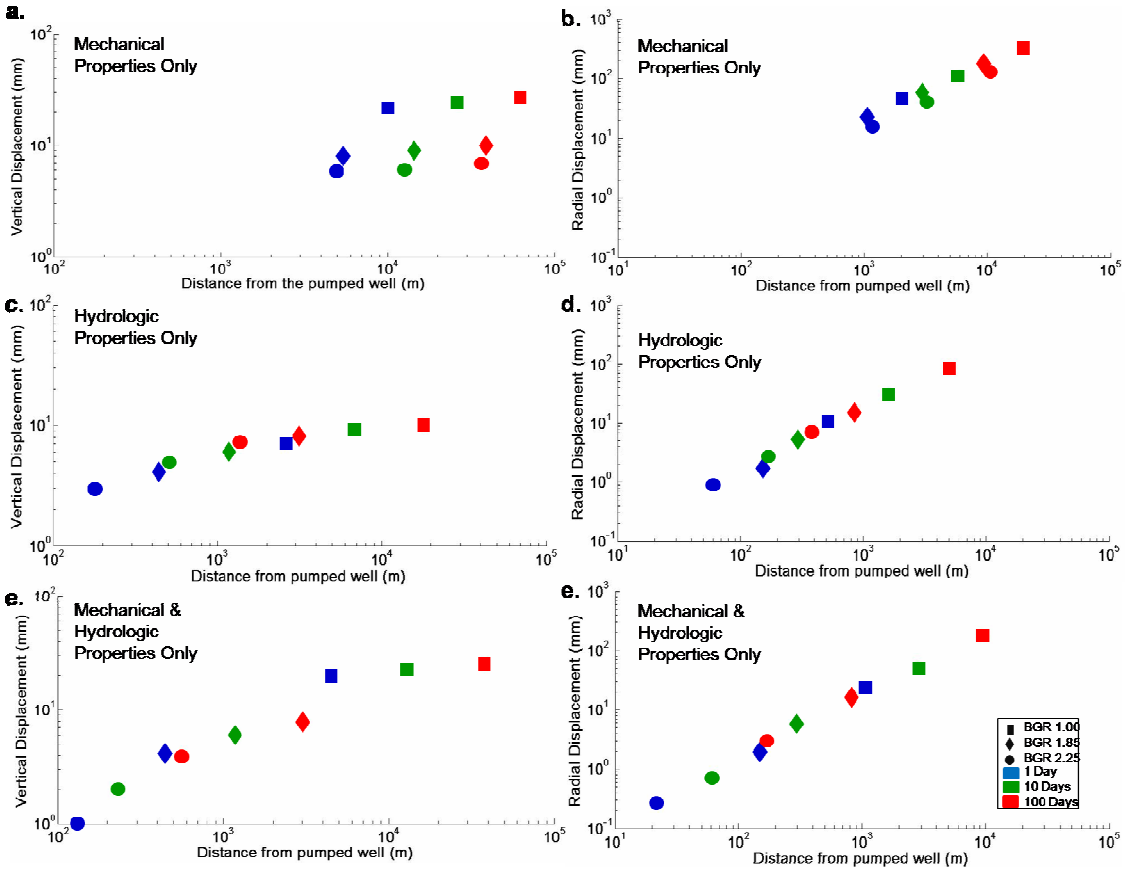

Figure 15. Vertical and radial deformation from the eight poroelastic models after 1, 10 and 100 days of pumping. **a)** Vertical displacement as a result of changing the shear modulus. **b)** Radial displacement as a result from only changing the mechanical properties. **c)** Vertical displacement as a result of changing only the hydraulic conductivity. **d)** Radial displacement results from changing only the hydrologic properties. **e)** Vertical displacement as a result of changing the shear modulus and hydrologic properties. **f)** Radial displacement results from changing the mechanical and hydrologic properties. Note the axis changes from the vertical to radial deformation plots.

CHAPTER 9

DISCUSSION

9.1 DEM Models

The two major implications of using DEM model for this research are 1) the DEM models prove to be a robust tool for isolating changes in elastic and inelastic mechanical behavior of granular porous media. 2) the BGRs of the DEM models appear to be a reliable method of correlating the behavior of the DEM models to the inherent properties of natural samples. The successful correlation of the DEM models to natural samples using the BGR, has implications for expanding this research to different cement and grain mineralogies. With this method of quantifying cementation in granular porous media we can eventually establish a quantitative relationship for a wide variety of cement (i.e. amount and mineralogy) and grain (i.e. size, shape, sorting and mineralogy) combinations.

Correlating the DEM models to natural samples may also prove useful for scaling the DEM model to three dimensional models and provide a better understanding of the intrinsic properties of the DEM models (e.g. pore space) (The three dimensional models will inherently have higher porosities because the grain will be supported in the third dimension.) As well as test the assumptions of the two dimensional DEM models (i.e. no plane strain). The three dimensional models will also provide us with a way of further

quantifying the amount of cement in the models because the bonds will have a length and width, as opposed the just a length as prescribed in the two dimensional models.

Preliminary steps are currently underway in preparation to preform ultrasonic velocity and triaxial deformation tests on natural samples to help understand differences between the natural samples and DEM models, as well as help further constrain input parameters of DEM models. Future work will also include an investigation of the influence of cement mineralogy on elastic and inelastic parameters.

9.2 Poroelastic Models

9.21 Implication of Results for Understanding Deformation in Aquifers

The three key implications of this research are 1) the parameterization continuum scale models in such a way as to capture meso-scale properties in a computationally reasonable manner. 2) the ability to quantify the effects of changes in the amount of cementation on fluid flow and deformation of granular porous media and 3) understand the importance of the competing roles of hydrologic and mechanical properties on aquifer deformation.

A key component of this research is the ability to scale the meso-scale results of the DEM model up to macro-scale by using the elastic parameters of the DEM models. This technique is revolutionary because DEM models have to be limited in size and elements in order to run in a reasonable amount of time. The continuum physics of the poroelastic models and the use of a finite elements code allows us to run macro-scale models in less time than it takes to run the meso-scale DEM models.

One limitation of this technique is the inability of the poroelastic models to capture the inelastic behavior of the macro-scale models. For the models used in this research we do not believe this is a problem because for each BGR the percent strain experienced by the poroelastic model is far less than the strain experienced by the DEM model before inelastic deformation occurs. For example, in the DEM models, the BGR 1.00 model experiences the most compression strain (0.022) before experiencing inelastic deformation. When compared to the maximum vertical and radial strain in the poroelastic models, BGR 1.00 experiences strains 2.54×10^{-4} and 2.012×10^{-4}, respectively. Since the strains in the poroelastic models are approximately two orders of magnitude smaller than the threshold of inelastic strain in the DEM models, the deformation associated with the strain in the poroelastic models is assumed to be elastic. However, for models with boundary conditions that allow strain in the inelastic realm (e.g. high pumping rates and low permeability) the physics of the poroelastic models may no longer be robust and alternative modeling techniques should be considered such as those that incorporate inelastic deformation (e.g. viscoelasticity and plasticity).

Even without incorporating inelastic deformation in to this study, this research demonstrates the variability in deformation due to cementation. By changing the mechanical and hydrologic properties for a single BGR simulation the maximum vertical and radial deformation varied over half an order of magnitude. Considering the relatively short amount of time modeled (100 days) and that aquifers are used for decades, a half order of magnitude difference in deformation is a significant range, which reiterates the importance of quantifying the mechanical and hydrologic input parameters.

While the magnitude of deformation is obviously sensitive to changes in mechanical and hydrologic properties the hydrologic properties are even more sensitive, as indicated by hydrologic properties' control on the magnitude of deformation and area influenced by deformation. With the range of hydrologic and mechanical properties prescribed to the models the region influenced by deformation varied by two orders of magnitude. This is significant because all of the values used in the models are well within the range of values that could be assumed for a generic poroelasticity model, which could allow for a two order of magnitude error. Understanding the influence of hydrologic properties on poroelastic modeling is applicable to multiple disciplines. As the need for oil increases and interest in geologic carbon sequestration grows the importance of understanding the role of fluid and gases in deformation will continue to grow too.

9.22 Influence of Boundary Conditions on Results

All of these models were run with a constant drawdown boundary condition to simulate a pumping well. While this technique is usefully for standardizing the amount of fluid removed from each model and simplifying the results, natural systems do not always work this way. Therefore, we ran sensitivity models to understand the influence of this boundary condition on the models. For the sensitivity models the outward flux was set at a constant pumping rate for the duration of the simulation. For these models a there was a larger range in the magnitude and area of deformation because the hydrologic properties played a greater role in controlling the region that experienced changes in fluid pressure.

CHAPTER 10

CONCLUSIONS

The meso-scale investigation revealed a direct correlation between BGR and mechanical response of simulated granular porous media. The BGRs are effective for correlating the amount of cement in the DEM models with quantitative amounts of cement in natural samples as well as correlating the effects of changes in the amount of cementation with changes in permeability.

At the macro-scale, changes in mechanical and hydrologic properties directly influence the magnitude and area of surface deformation. The significant difference in sensitivity of the system to the mechanical properties alone to the sensitivity of both mechanical and hydrologic properties demonstrates the importance of including hydrologic properties that are adjusted for changes in cementation in fluid storage and deformation studies. Also, the high values of radial deformation emphasizes the importance of considering three dimensional deformation in fluid flow and deformation studies.

This research has provided the framework for quantitative data on the effects of cementation on the mechanical and hydrologic properties of granular porous media. This research has implications for increased understanding of both groundwater aquifers and oil reservoirs as well as geologic carbon sequestration studies.

APPENDIX A

EFFECTS OF GRAIN GEOMETRY ON MECHANICAL RESPONSE AND BGR OF THE DEM MODELS

A1. Grain Packing

The size and geometry of the grains in the DEM models were altered to investigate the influence of various grain packings on the mechanical response of the DEM models. Three grain geometries were used to create different packing arrangements; ellipsoidal grains, circular grains and grains of mixed geometries (Figure A1). The domains were prescribed to obtain a similar range of grain diameters and approximately the same number of grains for each grain geometry. The slightly larger grain diameter and number of grains in the mixed grain geometry domain resulted in a larger overall domain area. The characterization for the three different grain geometries is listed in Table A1. Note that the reported porosity is the granular porosity; cementation is not considered in the porosity calculation. Also, the two dimensionality of the models creates an artificially low model porosity as compared to natural samples because the grains are not supported in the third dimension. The porosity is calculated by the DEM model.

Since the grain size and geometry control the packing arrangements and therefore the distance between the grains, the bond radius had to be varied for each grain geometry in order to obtain similar BGRs. The influence of packing on the BGR is readily observed when the bond radius is held constant. A bond radius of 0.1815 cm translates into BGRs of 2.25, 2.28 and 1.00 for the ellipsoidal, circular and mixed grain geometries,

respectively (Table A2). Understanding the effects of packing and grain distribution on bonding could have implications for understanding the tendencies of cementation in natural samples where the distance between grains may determine if the cement is grain bridging or just simply coating a grain. Simulating three different grain geometries with the same BGR also allow us to investigate the inherent strength of the different packings.

A2. Results for various grain geometries

The ellipsoidal grain simulations were consistently the most resilient, failing at higher stresses for each BGR then the circular or mixed grain geometries (Figure A2, A3 and Table 3A). Figure A3 elucidates the effects of the grain geometry on the mechanical response of all the grain geometries at a BGR of 2.25. The ellipsoidal grain geometry proves to be the stiffest packing, followed by the circular grain geometry and finally the mixed grain geometry. The consistently higher stiffness may reflect the increase in grain to grain contact and increased surface friction. While the circular and mixed grain simulations failed at lower stress, the model displayed larger changes in stiffness for each change in BGR than the ellipsoidal grain geometry simulations, suggesting the inherent strength of the packing influences the bulk elastic parameters and yield strength.

In general higher BGRs resulted in stiffer simulations and failure at smaller displacements. There is some variation caused by the slip-stick behavior seen in Figure A2.c. Regardless of the variations in grain size and shape and domain size the models experienced similar failure trends as shown in Figure A4.

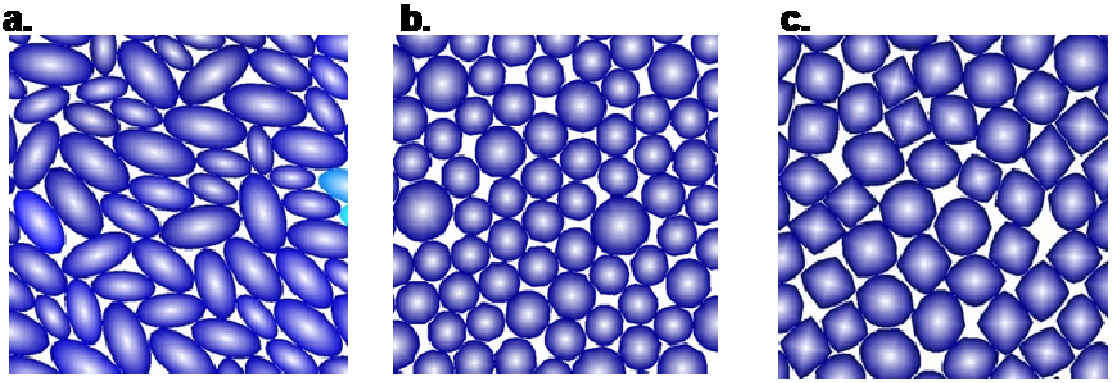

Figure A 1. Representative grain geometries for the **a)** ellipsoidal grains **b)** circular grains **c)** and mixed grains.

Table A 1. Characterization of the three grain geometry models.

Geometry	Grains	Mean Grain Diameter (m)	Domain Dimensions (m)	Porosity
Ellipsoidal	3060	0.0018	0.035 x 0.132	11.73%
Circular	3062	0.0017	0.053 x 0.134	14.07%
Mixed	3152	0.0023	0.085 x 0.151	13.66%

Table A 2. Comparison of the properties of various grain geometries.

Geometry	Bond Length	BGR	Number of Bonds
Ellipsoidal			
	0.1	0.50	1536
	0.117	1.00	3054
	0.15	1.85	5673
	0.1815	2.25	6896
Circular			
	0.1425	0.50	1558
	0.1476	1.00	3033
	0.161	1.85	5672
	0.178	2.25	6898
	0.1815	2.28	6988
Mixed			
	0.174	0.50	1715
	0.1815	1.00	3126
	0.195	1.83	5742
	0.23	2.25	7083

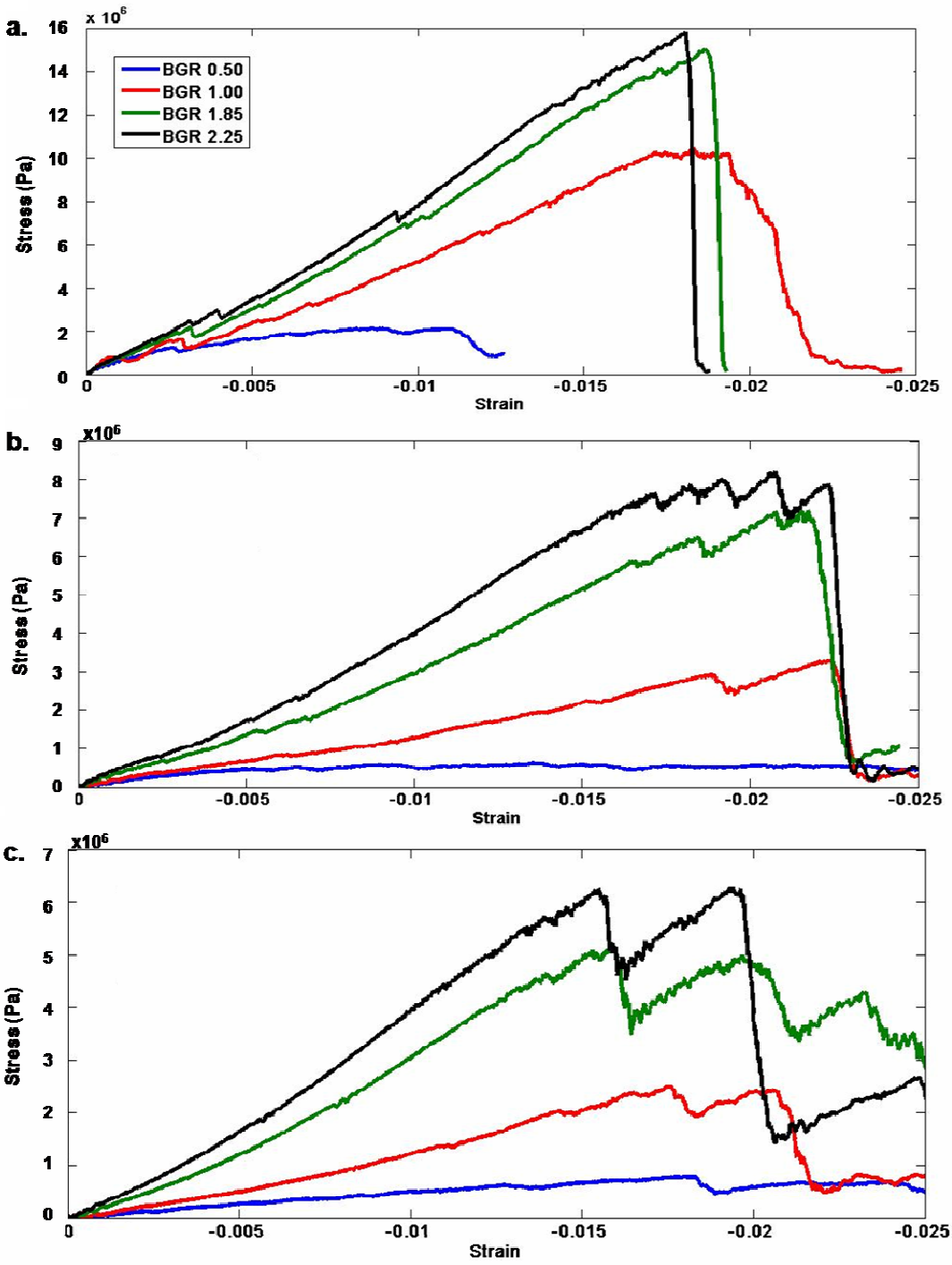

Figure A 2. Comparison of the stress-strain curves for the (a) ellipsoidal, (b) circular and (c) mixed grain geometries.

Table A 3. Inelastic and elastic results for all three grain geometries and each BGR.

Geometry	BGR	Yield Strength (Pa)	Young's Modulus (Pa)	Poisson's Ratio
Ellipsoidal				
	0.5	2.08E+06	2.58E+08	0.56
	1	1.01E+07	7.07E+08	0.46
	1.85	1.50E+07	9.33E+08	0.3
	2.25	1.58E+07	1.22E+09	0.27
Circular				
	0.5	6.76E+05	1.28E+08	0.63
	1	3.28E+06	1.81E+08	0.61
	1.85	7.82E+06	4.58E+08	0.43
	2.25	8.20E+06	5.57E+08	0.36
	2.28	8.44E+06	5.37E+08	0.35
Mixed				
	0.5	8.26E+05	4.24E+07	0.61
	1	2.50E+06	1.82E+08	0.53
	1.83	5.45E+06	3.93E+08	0.3
	2.25	6.70E+06	5.18E+08	0.3

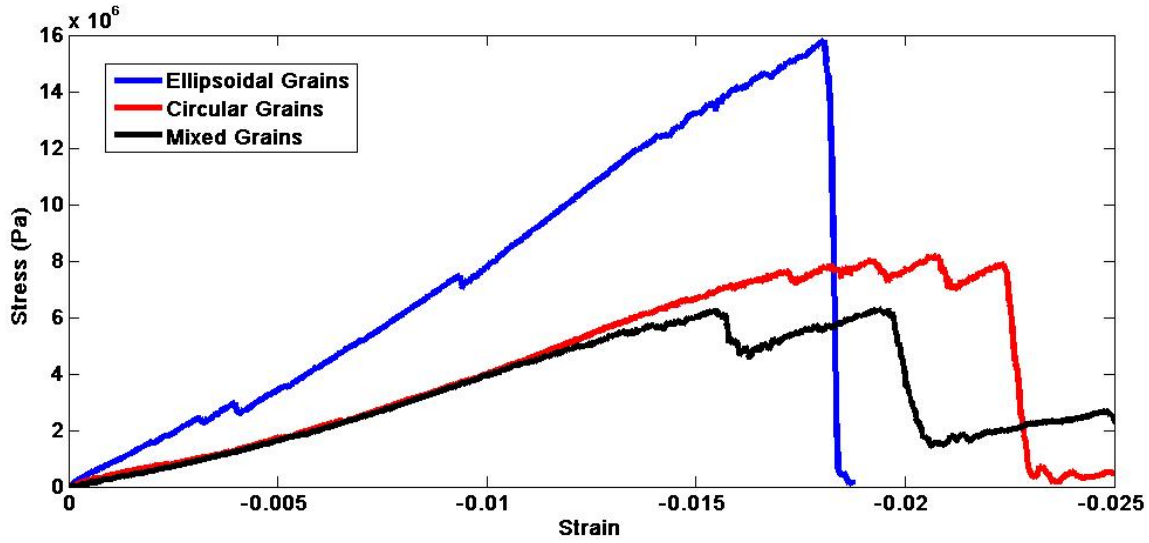

Figure A 3. Comparison of the ellipsoidal, circular and mixed grain geometry stress-strain data for BGR 2.25.

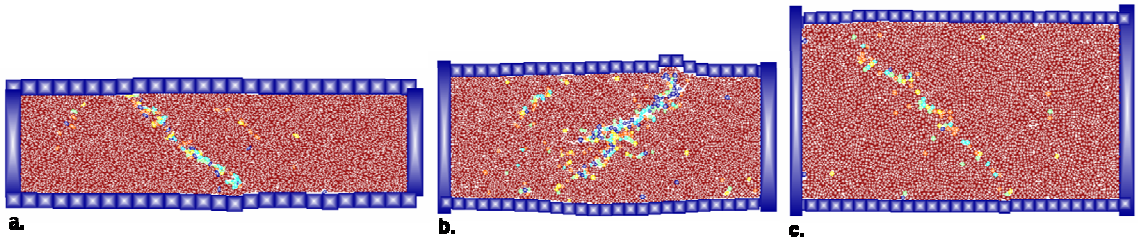

Figure A 4. Comparison of the deformation patterns for the ellipsoidal (a), circular (b) and mixed grain geometries (c).

APPENDIX B

POROELASTIC MODELS

B1. Model Validation

The models were validated by comparing the results from the analytical solution for the Theis equation and the results from the uncoupled poroelastic models. We compared the results from the poroelastic models to the calculated drawdown from the Theis equation at 0.1, 1.0, 100, and 1000 meters from the well at 1, 10 and 100 days. The calculated drawdown for the two methods is quite similar (Figure B1). The discrepancies could be attributed to the timestep taken by the model.

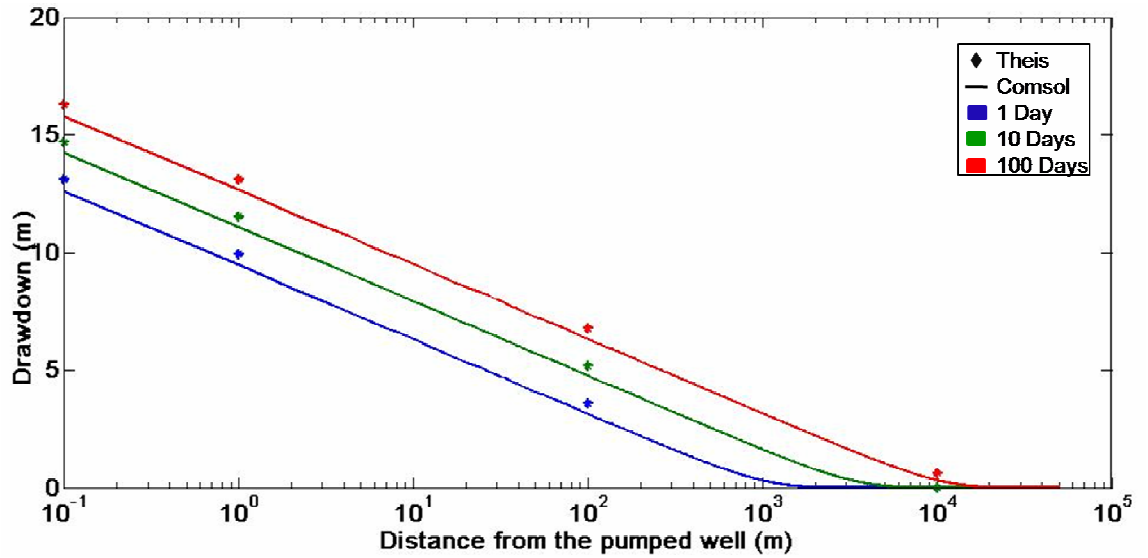

Figure B 1. Comparison of the drawdown in the uncoupled poroelastic models to the analytical Theis equation as a function of the distance from the pumped well.

Table B 1. Comparison of values of drawdown using the poroelastic models, the Theis equation and BiotII.

	Drawdown (m)								
	1 day			10 days			100 days		
Distance (m)	**Comsol**	**Theis**	**Biot**	**Comsol**	**Theis**	**Biot**	**Comsol**	**Theis**	**Biot**
0.1	7	13	7	9	14	8	10	16	9
1	7	10	6	8	11	6	10	13	7
100	3	3	2	6	5	3	7	6	4
10000	0	0	0	2	0	0	3	3	0

B2. Changes in drawdown trends from variation in hydromechanical properties

The influence of changes in the mechanical and hydrologic properties can also be seen by changes in hydraulic head as a function of distance from the pumped well (Figure B2). After 100 days of pumping, the poroelastic models in which only the mechanical properties were varied show at relative trend in the area influenced by fluid withdrawal. This drawdown cone from this set of models varies from the models that included changes in hydrologic properties in that the lowest BGR (1.00) resulted in the least amount of drawdown. This trend emphasizes the importance of the storage mechanism. The deformation allowed by the granular skeleton because of the low cement content forced fluid out of the formation, so even though fluid is being withdrawn the head still remains relatively high as compared to the higher cement cases.

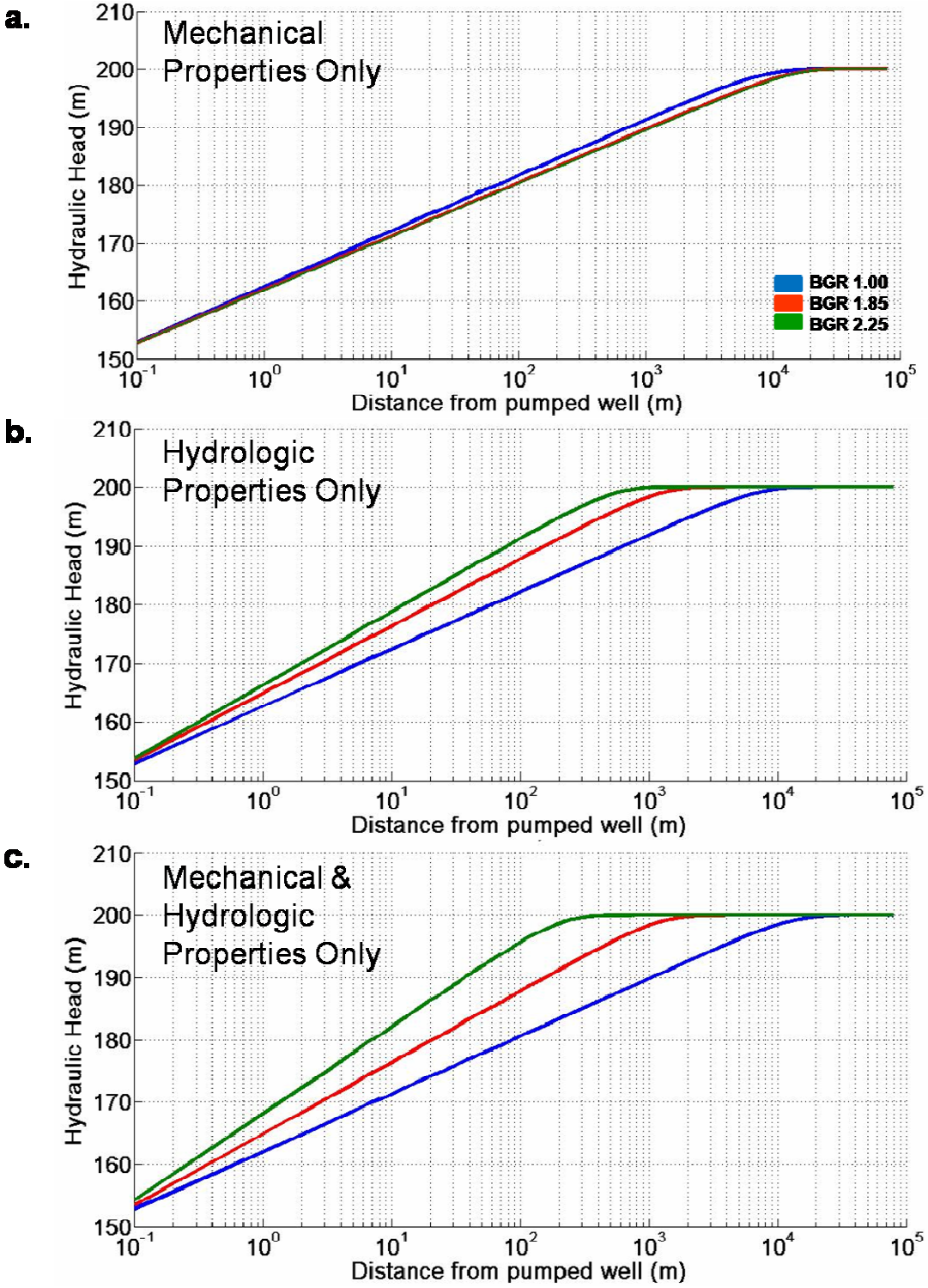

Figure B 2. Comparison of drawdown cones from the poroelastic simulations.

Table B 2. Raw data from the poroelastic models for the ellipsoidal grain geometry.

BCR	Altered Properties	Shear Modulus (Pa)	Permeability (m^2)	Porosity (%)	Z-displacement (mm)			location of 0 z-displacement (m)			R-displacement (mm)			location of max r-displacement (m)		
					1 day	10 days	100 days	1 day	10 day	100 days	1 day	10 days	100 days	1 day	10 days	100 days
1	Mechanical	7.0E+08	1.0E-13	15	22	24	27	9983	26260	62910	43	112	343	2043	5938	19540
	Hydrologic	9.3E+08	1.0E-12	25	20	22	25	4491	12960	38080	23	58	175	1038	2869	9455
	Mech. & Hydro.	7.0E+08	1.0E-12	25	7	9	10	2620	6731	17850	11	30	88	523	1596	5015
1.85	Mechanical	9.3E+08	1.0E-13	15	8	9	10	5461	14670	39580	21	55	165	1100	3054	9885
	Hydrologic	9.3E+08	3.0E-14	12	4	6	8	444	1174	3102	2	6	18	155	296	857
	Mech. & Hydro.	9.3E+08	3.0E-14	12	4	6	8	444	1174	3102	2	6	18	155	296	857
2.25	Mechanical	1.2E+09	1.0E-13	15	6	6	7	4977	12840	36060	17	45	137	1117	3203	10320
	Hydrologic	9.3E+08	9.0E-15	8	1	2	4	131	230	558	0.27	0.74	2.6	22	62	169
	Mech. & Hydro.	1.2E+09	9.0E-15	8	3	5	7	178	504	1370	1	3	8	61	170	379

BIBLIOGRAPHY

Ahmed, U., S. Crary, and G. Coates (1991), Permeability estimation: the various sources and their interrelationship, Journal of Petroleum Technology, 43, 578-87.

Berg, R., (1970), Method of determining permeability from reservoir rock properties, Gulf Coast Association of Geologic Society Transaction 20, 303-17.

Bloch, S. (1991), Empirical prediction of porosity and permeability in sandstones, AAPG Bulletin, 75, 1145-1160.

Boutt, D. F., B. K. Cook, B. J. O. L. McPherson, and J. R. Williams (2007), Direct simulation of fluid-solid mechanics in porous media using the discrete element and lattice-Boltzmann methods, *J. Geophys. Res.,* 112, B10209, doi:10.1029/2004JB003213.

Boutt, D. F., and B. J. O. L. McPherson (2002), Simulation of sedimentary rock deformation: Lab-scale model calibration and parameterization, Geophys. Res. Lett., 29(4), 1054, doi:10.1029/2001 GL013987.

Burbey, T. J. (1999) Effects of horizontal strain in estimating specific storage and compaction in confined and leaky aquifer systems, Hydrogeology Journal 7:521-532.

Bruno, M., and R. Nelson (1991), Microstructural analysis of the inelastic behavior of sedimentary rock, *Mech. Mater.*, 12, 95-118.

Campbell, C., P. Cleary, and M. Hopkins (1995), Large scale landslide simulations: Global deformation, velocities and basal friction, *J. Geophys. Res.* 100, 8267-8383.

Carman, P. C. (1937), Fluid flow through granular beds, Trans. Inst. Chem. Eng. London 15 150.

Carman, P. C. (1948), Some physical aspects of water flow in porous media, discuss. Faraday Soc. 3, 78.

Carman, P. C. (1956) The flow of gases through porous media. New York: Academic Press.

Cleary, P. W., and C. S. Campbell (1993), Self-lubrication for long runout landslides: Examination by computer simulation, *J. Geophys. Res*., 98(B12), 21,911-21,924.

Comsol multiphysics modeling guide. Comsol AB, 1994-2006.

Cook, B. K. (2001), A numerical framework for the direct simulation solid-fluid systems, Doctoral dissertation, Mass. Inst. Of Technol,. Cambridge.

Cooper, H. H., Jr. (1966). The equation of groundwater flow in fixed and deforming coordinates. *Journal of Geophysical Research* **71**, 4785-90.

Cundall, P. (1971), A computer model for simulating progressive, large scale movement in block rock systems, in *Rock Fracture*, vol 1, Int. Soc. For Rock Mech,. Lisbon, Portugal.

Cundall, P., and O. Strack (1979), A discrete element model for granular assemblies, *Geotechnique*, 29(1), 47-65.

Cundall, P., A. Drescher, and O. Strack (1982), Numerical experiments on granular assemblies: Measurements and observations, in *Deformation and Failure of Granular Materials,* edited by J. Jenkins and H. Luger, pp. 355-370, A. A. Balkema, Brookfield, Vt.

Fatt, I., 1958, Pore volume compressibilities of sandstone reservoir rocks, Petroleum Trans. AIME 213, 362-364.

Galloway, Devin L., Jones, David R., and Ingebritsen, S. E., Land subsidence in the United States. U.S. Dept. of the Interior, U.S. Geological Survey, 1999.

Green, D., and H. Wang (1990), Specific storage as a poroelastic coefficient, *Water Resour. Res*,. 26, 1631-1637.

Hall, H.N., 1953, Compressibility of reservoir rocks, Trans., AIME 198, 309-311.

Hazzard, J., P. F. Young, and S. Maxwell (2000), Micromechanical modeling of cracking and failure in brittle rocks*, J. Geophys. Res.,* 105, 16,683-16,697.

Helm, Donald, C. (1994), Horizontal aquifer movement in a Theis-Thiem confined system, *Water Resour. Res*,. 30, 953-964.

Jacob, C. E. (1940). On the flow of water in an elastic artesian aquifer. *Transactions American Geophysical Union* **21**, 574-86.

Jalalh, A. A. (2006), Compressibility of porous rocks: Part I. Measurements of Hungarian reservoir rock samples, *Acta Geophysica,* 54, 319-332, doi 10.2478/s11600-006-0025-8.

Kent, C. (2006), Discrete element simulation of bonded granular media, Master's Thesis, Univ. of NM, Albuquerque.

Kozeny, J. (1927), Über die kapillare Leitung des Wassers im Boden (Aufstieg, Versickerung und Anwendung auf die Bewässerung), Sitz. Ber. Akad. Wiss. Wien. Math. Nat. (Abt. IIa) 136a, 271-306.

Molenaar, N., J. Cyziene, and S. Sliaupa (2007), Quartz cementation mechanisms and porosity variation in Baltic Cambrian sandstones, Sedimentary geology, 195, 135-159.

Morgan, J. (1999), Numerical simulations of granular shear zones using the distinct element method 2. Effects of grain size distribution and intergrain friction on mechanic behavior, *J. Geophys. Res*., 104, 2721-2732.

Morgan, J., and M. Boettcher (1999), Numerical simulations of granular shear zones using the distinct element method 1. Shear zone kinematics and the micromechanics of localization, *J. Geophys. Res.,* 104, 2703-2719.

Mower T., and D., Budd, (1996), Quantification of porosity and permeability reduction due to calcite cementation using computer-assisted petrographic image analysis techniques, AAPG Bulletin, 80, 309-322.

New England Research. New England Reseach -About NER. 2003-2008 http://nersolutions.com/site/ (Dec., 29, 2008).

Pande, G., G. Beer, and J. Williams (1990), Numerical Modeling in Rock Mechanics, John Wiley, New York.

Pape, H., C. Clauser and J. Iffland (2000). Variation of permeability with porosity in sandstone diagenesis interpreted with a fractal pore space model, Pure appl. Geophys., 157, 603-619.

PFC2d, theory and background. Itasca Consulting Group, Inc., Minneapolis, Minnesota, 1999.

Potyondy, D.O., and P. A. Cundall (2004), A bonded-grain model for rock, *Int. J. Rock Mech. Min. Sci.* 41(8), 1329-1364.

Potyondy, D.O., P. A. Cundall, and C. Lee (1996), Modeling rock using bonded assemblies of circular grains, in *Rock Mechanics: Took and Techniques: Second North American Rock Mechanics Symposium (NARMS),* editied by M. Aubertinin, F. Hassani, and H. Mitri, pp. 1937-1944, A. A. Balkema, Rotterdam, Netherlands.

Rege, N. (1996), Computational modeling of ranular materials, Doctoral dissertation, Mass. Inst. Of Technol., Cambridge.

Terzaghi, K (1923). Die Berechnung der Durchlässigkeitziffer des Tones aus dem Verlauf der Hydrodymanischen Spannungserscheinungen [The computation of permeability of clays from the progress of hydrodynamic strain]. *Akademie der Wissenschaften in Wien, Sitzungsberichte, Mathematisch-Naturwissenschaftliche Klasse, Part IIa* ***132****, 125-38.*

Terzaghi, K. (1925). *Erdbaummechanic.* Vienna: Franz Deuticke.

Terzaghi, K. (1943), Theoretical Soil Mechanics, John Wiley, New York.

Valliappan, S., J. Yazdi, and C. Zhao (1995), Analytical solution for two-dimensinal dynamic consolidation in frequency domain, Int. J. Numer. Anal. Methods Geomech., 19, 663-682.

Wang, H. (2000), Theory of Linear Poroelasticity: With Applications to Geomechanics and Hydrogeology, Princeton Univ. Press, Prinction, N.J.

Williams, J. R., and N. Rege (1997), The development of circulation cell structures in granular materials undergoing compression*, Powder Technol.,* 90, 187-194.